Atmos. Chem. Phys. Discuss., 8, 2429–2512, 2008
www.atmos-chem-phys-discuss.net/8/2429/2008/

Atmospheric Chemistry and Physics Discussions

Validation of HNO_3, $ClONO_2$, and N_2O_5 from the Atmospheric Chemistry Experiment Fourier Transform Spectrometer (ACE-FTS)

M. A. Wolff[1], T. Kerzenmacher[1], K. Strong[1], K. A. Walker[1,2], M. Toohey[1], E. Dupuy[2], P. F. Bernath[2,3], C. D. Boone[2], S. Brohede[4], V. Catoire[5], T. von Clarmann[6], M. Coffey[7], W. H. Daffer[8], M. De Mazière[9], P. Duchatelet[10], N. Glatthor[6], D. W. T. Griffith[11], J. Hannigan[7], F. Hase[6], M. Höpfner[6], N. Huret[5], N. Jones[11], K. Jucks[12], A. Kagawa[13, 14], Y. Kasai[14], I. Kramer[6], H. Küllmann[15], J. Kuttippurath[15,*], E. Mahieu[10], G. Manney[16,17], C. McLinden[18], Y. Mébarki[5], S. Mikuteit[6], D. Murtagh[4], C. Piccolo[19], P. Raspollini[20], M. Ridolfi[21], R. Ruhnke[6], M. Santee[16], C. Senten[9], D. Smale[22], C. Tétard[23], J. Urban[4], and S. Wood[22]

[1]Department of Physics, University of Toronto, Toronto, Ontario, Canada
[2]Department of Chemistry, University of Waterloo, Waterloo, Ontario, Canada
[3]Department of Chemistry, University of York, York, UK
[4]Department of Radio and Space Science, Chalmers University of Technology, Gothenburg, Sweden
[5]Laboratoire de Physique et Chimie de L'Environment CNRS – Université d'Orléans, Orléans, France

[6]Forschungzentrum Karlsruhe and University of Karlsruhe, Institute for Meteorology and Climate Research, Karlsruhe, Germany
[7]National Center for Atmospheric Research (NCAR), Boulder, CO, USA
[8]Columbus Technologies Inc., Pasadena, CA, USA
[9]Belgian Institute for Space Aeronomy, Brussels, Belgium
[10]Institute of Astrophysics and Geophysics, University of Liège, Liège, Belgium
[11]School of Chemistry, University of Wollongong, Wollongong, Australia
[12]Harvard-Smithsonian Center for Astrophysics, Cambridge, MA, USA
[13]Fujitsu FIP Corporation, Tokyo, Japan
[14]Environmental Sensing and Network Group, National Institute of Information and Communications Technology (NICT), Tokyo, Japan
[15]Institute of Environmental Physics, University of Bremen, Bremen, Germany
[16]Jet Propulsion Laboratory, California Institute of Technology, Pasadena, CA, USA
[17]New Mexico Institute of Mining and Technology, Socorro, NM, USA
[18]Environment Canada, Toronto, Ontario, Canada
[19]Atmospheric, Oceanic and Planetary Physics, University of Oxford, Oxford, UK
[20]Institute of Applied Physics "Nello Carrara", National Research Center (CNR), Firenze, Italy
[21]Dipartimento di Chimica Fisica e Inorganica, Università di Bologna, Bologna, Italy
[22]National Institute of Water and Atmospheric Research Ltd., Central Otago, New Zealand
[23]Laboratoire d'Optique Atmosphérique, Université des Sciences et Technologies de Lille, Villeneuve d'Ascq, France
*now at: LMD/CNRS Ecole polytechnique, Palaiseau Cedex, France

Received: 4 December 2007 – Accepted: 11 December 2007 – Published: 8 February 2008

Correspondence to: M. A. Wolff (mwolff@atmosp.physics.utoronto.ca)

Abstract

The Atmospheric Chemistry Experiment (ACE) satellite was launched on 12 August 2003. Its two instruments measure vertical profiles of over 30 atmospheric trace gases by analyzing solar occultation spectra in the ultraviolet/visible and infrared wavelength regions. The reservoir gases HNO_3, $ClONO_2$, and N_2O_5 are three of the key species provided by the primary instrument, the ACE Fourier Transform Spectrometer (ACE-FTS). This paper describes the ACE-FTS version 2.2 data products, including the N_2O_5 update, for the three species and presents validation comparisons with available observations. We have compared volume mixing ratio (VMR) profiles of HNO_3, $ClONO_2$, and N_2O_5 with measurements by other satellite instruments (SMR, MLS, MIPAS), aircraft measurements (ASUR), and single balloon-flights (SPIRALE, FIRS-2). Partial columns of HNO_3 and $ClONO_2$ were also compared with measurements by ground-based Fourier Transform Infrared (FTIR) spectrometers. Overall the quality of the ACE-FTS v2.2 HNO_3 VMR profiles is good from 18 to 35 km. For the statistical satellite comparisons, the mean absolute differences are generally within ±1 ppbv (±20%) from 18 to 35 km. For MIPAS and MLS comparisons only, mean relative differences lie within ±10% between 10 and 36 km. ACE-FTS HNO_3 partial columns (~15–30 km) show a slight negative bias of −1.3% relative to the ground-based FTIRs at latitudes ranging from 77.8° S–76.5° N. Good agreement between ACE-FTS $ClONO_2$ and MIPAS, using the Institut für Meteorologie und Klimaforschung and Instituto de Astrofísica de Andalucía (IMK-IAA) data processor is seen. Mean absolute differences are typically within ±0.01 ppbv between 16 and 27 km and less than +0.09 ppbv between 27 and 34 km. The $ClONO_2$ partial column comparisons show varying degrees of agreement, depending on the location and the quality of the FTIR measurements. Good agreement was found for the comparisons with the midlatitude Jungfraujoch partial columns for which the mean relative difference is 4.7%. ACE-FTS N_2O_5 has a low bias relative to MIPAS IMK-IAA, reaching −0.25 ppbv at the altitude of the N_2O_5 maximum (around 30 km). Mean absolute differences at lower altitudes (16–27 km) are typically

ACPD

8, 2429–2512, 2008

−0.05 ppbv for MIPAS nighttime and ±0.02 ppbv for MIPAS daytime measurements.

1 Introduction

This is one of two papers describing the validation of NO_y species measured by the Atmospheric Chemistry Experiment (ACE) through comparisons with coincident measurements. The total reactive nitrogen, or NO_y, family consists of NO_x (NO + NO_2) + all oxidized nitrogen species:

$$[NO_y] = [NO] + [NO_2] + [NO_3] + [HNO_3] + [HNO_4] + [ClONO_2] + [BrONO_2] + 2[N_2O_5]. \quad (1)$$

The ACE-Fourier Transform Spectrometer (ACE-FTS) measures all of these species, with the exception of NO_3 and $BrONO_2$ (Bernath et al., 2005), while the ACE-Measurement of Aerosol Extinction in the Stratosphere and Troposphere Retrieved by Occultation (ACE-MAESTRO) also measures NO_2 (McElroy et al., 2007). The species NO, NO_2, HNO_3, $ClONO_2$, and N_2O_5 are five of the 14 primary target species for the ACE mission, while HNO_4 is a research product. In this study, the quality of the ACE-FTS version 2.2 nitric acid (HNO_3), chlorine nitrate ($ClONO_2$), and ACE-FTS version 2.2 dinitrogen pentoxide (N_2O_5) update is assessed prior to its public release. A companion paper by Kerzenmacher et al. (2007) provides an assessment of the ACE-FTS v2.2 nitric oxide (NO) and nitrogen dioxide (NO_2), and of the ACE-MAESTRO v1.2 NO_2. Validation of ACE-FTS v2.2 measurements of nitrous oxide (N_2O), the source gas for NO_y, is discussed by Strong et al. (2007).

The three molecules HNO_3, $ClONO_2$, and N_2O_5 are important reservoir species for nitrogen and chlorine in the stratosphere and therefore play an important role in stratospheric ozone chemistry. They can sequester the more reactive NO_x species, thereby reducing ozone destruction via fast catalytic cycles (Solomon, 1999; Brasseur and Solomon, 2005). NO_x/NO_y partitioning is largely determined by ozone and aerosol

concentrations (e.g., Salawitch et al., 1994; Solomon et al., 1996). HNO_3 is the dominant form of NO_y in the lower stratosphere, and is produced from NO_x by the reaction:

$$NO_2 + OH + M \rightarrow HNO_3 + M \quad \text{(R1)}$$

where M is a third body that remains unchanged under the reaction. HNO_3 is chemically destroyed by photolysis and oxidation by OH:

$$HNO_3 + h\nu \rightarrow OH + NO_2 \quad \text{(R2)}$$

$$HNO_3 + OH \rightarrow NO_3 + H_2O. \quad \text{(R3)}$$

Both processes make comparable contributions to HNO_3 loss in the lower stratosphere. At higher altitudes, Reaction (R3) becomes gradually more important and dominates the HNO_3 loss mechanisms in the upper stratosphere (Dessler, 2000).

$ClONO_2$ is also produced from NO_x by reaction with ClO:

$$ClO + NO_2 + M \rightarrow ClONO_2 + M \quad \text{(R4)}$$

and is photolyzed at ultraviolet wavelengths to create either $Cl + NO_3$, or $ClO + NO_2$.

N_2O_5 is created through the reaction:

$$NO_2 + NO_3 + M \rightarrow N_2O_5 + M. \quad \text{(R5)}$$

Because of the extremely low abundances of NO_3 during the day, this process occurs at night (Dessler, 2000). N_2O_5 is mainly destroyed by photolysis (more than 90%) and collisional decomposition, to generate NO_3 and either NO_2 or NO + O.

During polar winter, the conversion of NO_x and ClO to HNO_3, $ClONO_2$, and N_2O_5 reduces the chemical destruction of ozone. However, in the presence of polar stratospheric clouds (PSCs), $ClONO_2$ and N_2O_5 can undergo heterogeneous reactions with H_2O and HCl to create HNO_3 and release chlorine into chemically active forms. HNO_3

can, in turn, be removed from the gas phase through sequestration on the PSCs, and subsequently lost through sedimentation of large PSC particles. This process of denitrification effectively removes NO_y from the stratosphere, thereby suppressing Reaction (R4), and redistributes it to lower altitudes where the PSCs evaporate (e.g., Toon et al., 1986; Waibel et al., 1999). Hydrolysis of N_2O_5 can also occur on sulphuric acid aerosols, thereby affecting both HNO_3 concentrations and the ozone budget at mid-latitudes (Hofmann and Solomon, 1989).

Of the three species that are the focus of this work, HNO_3 has been the most widely measured. The first measurements of HNO_3 in the stratosphere were made by Murcray et al. (1968), and were followed by the first space-based measurements made by the Limb Infrared Monitor of the Stratosphere (LIMS) on Nimbus 7 (Gille and Russell, 1984; Gille et al., 1984). Regular ground-based Fourier transform infrared spectrometer (FTIR) measurements of HNO_3 were started in 1980 at the National Solar Observatory McMath solar telescope facility on Kitt Peak, Arizona, USA and in 1986 at the International Scientific Station of the Jungfraujoch (ISSJ) in the Swiss Alps (Rinsland et al., 1991). Since then, other stations have performed continuous FTIR measurements of HNO_3, most of them as part of the Network for the Detection of Atmospheric Composition Change (NDACC, http://www.ndacc.org). HNO_3 was measured during a series of Space Shuttle missions by the Atmospheric Trace MOlecule Spectroscopy (ATMOS) instrument, flown four times between 1985 and 1994 (Abrams et al., 1996; Gunson et al., 1996; Irion et al., 2002), by the CRyogenic InfraRed Radiance Instrumentation for Shuttle (CIRRIS 1A) (Bingham et al., 1997) in 1991, and by the CRyogenic Infrared Spectrometers and Telescopes for the Atmosphere (CRISTA) in 1994 (Offermann et al., 1999; Riese et al., 1999). With the launch of the Upper Atmosphere Research Satellite (UARS) in 1991, longer-term global distributions of HNO_3 were retrieved by the Cryogenic Limb Array Etalon Spectrometer (CLAES) (Roche et al., 1993, 1994; Kumer et al., 1996a), the Improved Stratospheric And Mesospheric Sounder (ISAMS) (Taylor et al., 1993, 1994, 1995), and the Microwave Limb Sounder (MLS) (Santee et al., 1999, 2004; Waters et al., 2006). The latter provides the most extensive

HNO_3 dataset to date. More recently, the Improved Limb Atmospheric Spectrometer (ILAS) on the Advanced Earth Observing Satellite (ADEOS) (Koike et al., 2000; Irie et al., 2002; Nakajima et al., 2002) and ILAS-II on ADEOS-II (Irie et al., 2006) both measured HNO_3 using infrared solar occultation.

In addition to the ACE-FTS, there are currently four satellite instruments measuring HNO_3. The Sub-Millimetre Radiometer (SMR) on Odin has been in orbit since 2001 (Murtagh et al., 2002; Urban et al., 2005), and the Michelson Interferometer for Passive Atmospheric Sounding (MIPAS) on Envisat, since 2002 (Mengistu Tsidu et al., 2005; Stiller et al., 2005; Wang et al., 2007a,b; Fischer et al., 2007). The Aura satellite, launched in 2004, carries another MLS (Waters et al., 2006; Santee et al., 2007) and the HIgh Resolution Dynamics Limb Sounder (HIRDLS) (Gille et al., 2007; Kinnison et al., 2007). These instruments are described in more detail below, in the context of comparisons with ACE-FTS.

Stratospheric $ClONO_2$ was first measured by Murcray et al. (1979) and Rinsland et al. (1985) using solar infrared absorption spectroscopy from a balloon platform. Zander and Demoulin (1988) reported on the retrieval of $ClONO_2$ column densities from FTIR measurements at the mountain station of the Jungfraujoch. Today, many of the FTIRs affiliated with NDACC perform $ClONO_2$ measurements. $ClONO_2$ was measured from space by ATMOS during all four Space Shuttle missions using infrared solar occultation spectroscopy (Zander et al., 1986; Rinsland et al., 1994, 1985, 1996; Zander et al., 1996) and by CRISTA using observations of infrared thermal emission (Offermann et al., 1999; Riese et al., 1999). CLAES was the only instrument on UARS able to detect $ClONO_2$, and it provided global profiles between October 1991 and May 1993 (Mergenthaler et al., 1996). It was followed by ILAS, which measured $ClONO_2$ from October 1996 to June 1997 (Nakajima et al., 2006), providing the first high-latitude coverage, and by ILAS-II from January to October 2003 (Wetzel et al., 2006). Currently, MIPAS is the only instrument, other than ACE-FTS, which is in orbit and measuring $ClONO_2$; Höpfner et al. (2007) describe validation of the profiles retrieved using the Institut für Meteorologie und Klimaforschung and Instituto de Astrofísica de Andalucía

ACPD
8, 2429–2512, 2008

(IMK-IAA) scientific data processor.

Spectroscopic measurements of N_2O_5 are difficult due to the presence of interfering species and aerosol in the 1240 cm^{-1} band that is typically used for retrievals. The first detection was by King et al. (1976); for a review of early efforts to measure N_2O_5 from the ground and balloons, see Roscoe (1991). Like $ClONO_2$, stratospheric N_2O_5 has been detected from space by ATMOS (Abrams et al., 1996; Gunson et al., 1996), CRISTA (Riese et al., 1997, 1999), CLAES (Kumer et al., 1996b, 1997), ILAS (Yokota et al., 2002; Oshchepkov et al., 2006), and ILAS-II (Wetzel et al., 2006). In addition, ISAMS, which operated on UARS from October 1991 to July 1992, detected N_2O_5 using pressure modulated radiometry (Taylor et al., 1993; Smith et al., 1996; Kumer et al., 1997). MIPAS is again the only instrument, other than ACE-FTS, which is currently measuring N_2O_5 from space (Mengistu Tsidu et al., 2004).

To date, ACE-FTS v2.2 HNO_3 volume mixing ratio profiles have been compared with data from the following satellite instruments: MIPAS ESA (Wang et al., 2007a), MIPAS IMK-IAA (Wang et al., 2007b), Aura-MLS (Froidevaux et al., 2006; Toohey and Strong, 2007; Santee et al., 2007), and HIRDLS (Kinnison et al., 2007). Additionally, they have been compared to balloon-borne measurements carried out during the Middle Atmosphere Nitrogen TRend Assessment (MANTRA) mission (Toohey et al., 2007). Mahieu et al. (2005) compared ACE-FTS v.1.0 $ClONO_2$ with ground-based measurements at northern latitudes and ACE-FTS v2.2 $ClONO_2$ profiles have been included in the validation of MIPAS IMK-IAA data products (Höpfner et al., 2007).

The objective of this validation exercise is to assess the quality of the current ACE-FTS data (v2.2 with updates for O_3, N_2O_5, and HDO). In this study, we compare the ACE-FTS v2.2 HNO_3 and $ClONO_2$ data and the ACE-FTS v2.2 N_2O_5 update data through comparisons with coincident measurements. The paper is organized as follows. In Sect. 2, the ACE mission and the retrievals of these three species are briefly described. Section 3 summarizes the validation methodology adopted. In Sect. 4, the results of vertical profile comparisons with the SMR, MLS, and MIPAS satellite instruments are discussed. Section 5 focuses on the results of comparisons with data from

ACPD
8, 2429–2512, 2008

the ASUR (Airborne SUbmillimeter wave Radiometer) aircraft flights and from the SPIRALE (SPectroscopie Infra-Rouge d'Absorption par Lasers Embarqués) and FIRS-2 (Far-InfraRed Spectrometer-2) balloon flights. Partial column comparisons with a network of ground-based FTIRs are presented in Sect. 6. Finally, the results are summarized and conclusions regarding the quality of the HNO_3 (v2.2), $ClONO_2$ (v2.2), and N_2O_5 (v2.2 update) data are given in Sect. 7.

2 ACE-FTS instrument description and data analysis

The Atmospheric Chemistry Experiment was launched on 12 August 2003. ACE is a Canadian-led satellite mission, also known as SCISAT, which carries two instruments, the ACE-FTS (Bernath et al., 2005) and the Measurement of Aerosol Extinction in the Stratosphere and Troposphere Retrieved by Occultation (ACE-MAESTRO) (McElroy et al., 2007). Both instruments record solar occultation spectra, ACE-FTS in the infrared (IR), and MAESTRO in the ultraviolet-visible(vis)-near-IR, from which vertical profiles of atmospheric trace gases, temperature, and atmospheric extinction are retrieved. In addition, a two channel near-IR-vis imager (ACE-IMAGER) provides profiles of atmospheric extinction at 0.525 and 1.02 μm (Gilbert et al., 2007). The SCISAT spacecraft is in a circular orbit at 650-km altitude, with a 74° inclination angle (Bernath et al., 2005), providing up to 15 sunrise and 15 sunset solar occultations per day. The choice of orbital parameters results in coverage from 85° S to 85° N with an annually repeating pattern, and a sampling frequency that is greatest over the Arctic and Antarctic. The primary scientific objective of the ACE mission is to understand the chemical and dynamical processes that control the distribution of ozone in the stratosphere and upper troposphere, particularly in the Arctic (Bernath et al., 2005; Bernath, 2006, and references therein).

ACE-FTS measures atmospheric spectra between 750 and 4400 cm^{-1} (2.2–13 μm) at 0.02 cm^{-1} resolution (Bernath et al., 2005). Profiles as a function of altitude for pressure, temperature, and over 30 trace gases are retrieved from ACE-FTS measure-

ments. The details of ACE-FTS data processing are described by Boone et al. (2005). Briefly, a non-linear least squares global fitting technique is employed to analyze selected microwindows (0.3–30 cm^{-1}-wide portions of the spectrum containing spectral features for the target molecule). The analysis approach does not employ constraints from a priori information (i.e., it is not an optimal estimation approach). Prior to performing volume mixing ratio (VMR) retrievals, pressure and temperature, as a function of altitude, are determined through the analysis of CO_2 lines in the spectra.

Issues have been identified in some ACE-FTS profiles and these have been flagged as Do Not Use (DNU). A continuously updated list of the DNU profiles and other data issues can be found at https://databace.uwaterloo.ca/validation/data_issues.php.

The ACE-FTS instrument collects measurements every 2 s, which yields a typical altitude sampling of 3–4 km within an occultation, neglecting the effects of refraction that compress the spacing at low altitudes. Note that this altitude spacing can range from 1.5–6 km, depending on the geometry of the satellite's orbit for a given occultation. The actual altitude resolution achievable with the ACE-FTS is limited to about 3–4 km, as a consequence of the instrument's field-of-view (1.25-mrad-diameter aperture and 650-km altitude). Atmospheric quantities are retrieved at the measurement heights. It should be noted that no diurnal corrections have been performed for any molecule retrieved from the ACE-FTS observations. For the purpose of generating calculated spectra (i.e., performing forward model calculations), quantities are interpolated from the measurement grid onto a standard 1-km grid using piecewise quadratic interpolation. The comparisons in this study were performed using the 1-km grid data. Forward model calculations employ the spectroscopic constants and cross section measurements from the HITRAN 2004 line list (Rothman et al., 2005).

The precision of the ACE-FTS VMRs is defined as the 1σ statistical fitting errors from the least-squares process, assuming a normal distribution of random errors (Boone et al., 2005).

2.1 HNO_3

ACE-FTS v2.2 microwindows for HNO_3 lie in the regions from 867–880 cm^{-1} and 1691.5–1728.6 cm^{-1}, used at altitudes from 5 to 37 km. A total of 12 microwindows are used in the retrievals. Interferences in the microwindow set include H_2O, O_3, N_2O, CH_4, CFC−12, and OCS. The interferers H_2O, O_3, N_2O, and CH_4 are retrieved simultaneously with HNO_3. OCS is fixed to the results of an earlier retrieval step. The contribution of CFC-12 in the microwindows contains no structure, and so is accounted for with the baseline (scale and slope) parameters in the fitting routine.

There is a discrepancy between the spectroscopic constants from HITRAN 2004 in the two HNO_3 regions (one near 900 cm^{-1} and the other band near 1700 cm^{-1}) used in the ACE-FTS retrievals. Figure 1 shows the difference between using a set of microwindows near 900 cm^{-1} versus a set of microwindows near 1700 cm^{-1}. The profiles shown are an average of 100 occultations. The discrepancy between intensities in the two bands appears to be in the range of 5 to 10%. Note that both regions are required in the retrieval because the region near 900 cm^{-1} is the only source of information at the lowest altitudes (below 10 km), while the 1700 cm^{-1}-band provides the only information at the highest altitudes (above 35 km). Both regions contribute information for the retrieval between 10 and 35 km. One consequence of this discrepancy is that retrieved HNO_3 VMR profiles could be noisier than they should be below 12 km. Future versions of ACE-FTS processing will scale the intensities in the band near 1700 cm^{-1} to achieve internal consistency between the two bands.

We have examined the fitting errors for the ACE-FTS HNO_3 profiles used in the comparisons with MLS (Sect. 4.2), and found that the median value is <5% from 10 to 35 km.

ACPD
8, 2429–2512, 2008

EGU

2.2 $ClONO_2$

ACE-FTS v2.2 $ClONO_2$ retrievals employ two microwindows containing Q-branches for the molecule. The first microwindow is centered at 780.15 cm^{-1} with a width of 0.6 cm^{-1}, and is used over the altitude range 12 to 20 km. The second microwindow is centered at 1292.6 cm^{-1} with a width of 1.6 cm^{-1}, and extends over the altitude range 18 to 35 km. Interferences in the microwindows include $^{12}CH_4$, $^{13}CH_4$, CH_3D, $^{14}N_2^{16}O$, $^{14}N^{15}N^{16}O$, $^{15}N^{14}N^{16}O$, H_2O, HDO, HNO_3, $^{16}O^{12}C^{18}O$, $^{16}O^{12}C^{17}O$, $^{16}O^{13}C^{18}O$, O_3, and a minor contribution from H_2O_2. Interfering species retrieved are O_3, HNO_3, CH_4, and N_2O. A single profile is used for all isotopologues of CH_4 and a single profile is used for all isotopologues of N_2O, even though different isotopologues of a molecule can have different VMR profiles. H_2O and HDO are fixed to the results of previous retrievals, and the CO_2 isotopologues use the VMR profile associated with the main isotopologue of CO_2. The contribution from H_2O_2 is calculated from a standard VMR profile for the molecule. The microwindow providing information at low altitudes (centered at 780.15 cm^{-1}) has a relatively poor signal-to-noise ratio in the ACE-FTS spectra, 40:1 as compared to 350:1 for the microwindow centered at 1292.6 cm^{-1}. Thus, noise on the retrieved VMR profile increases significantly below 18 km.

The median fitting errors of the ACE-FTS $ClONO_2$ profiles (from the same group of profiles as used for the examination of HNO_3 fitting errors) are ~40% at 14 km, below 10% from 20 to 30 km, and increasing to ~20% at 35 km.

2.3 N_2O_5

The spectral region analyzed for N_2O_5 retrievals ranges from 1210 to 1270 cm^{-1} and is divided into two windows of width 30 cm^{-1} each. The altitude range for the retrieval is from 15 to 40 km. Interferences in the spectral region include $^{12}CH_4$, $^{13}CH_4$, CH_3D, $^{14}N_2^{16}O$, $^{14}N^{15}N^{16}O$, $^{15}N^{14}N^{16}O$, $^{14}N^{14}N^{18}O$, $^{14}N^{14}N^{17}O$, $H_2^{16}O$, $H_2^{18}O$, HDO, HNO_3, $^{16}O^{12}C^{18}O$, $^{16}O^{12}C^{17}O$, O_3, COF_2, and a minor contribution from H_2O_2. Single pro-

files are retrieved for H_2O, CO_2, CH_4, and N_2O, neglecting differences in VMR profiles for different isotopologues. HDO, O_3, HNO_3, and COF_2 are fixed to the results of previous retrievals, and H_2O_2 is calculated from a standard VMR profile for the molecule. N_2O_5 uses the broadest wavenumber range of any molecule retrieved from the ACE-FTS data. During the original ACE-FTS v2.2 N_2O_5 retrievals, array overflows occurred during the retrieval process, not significant enough to cause the software to crash or to trigger any obvious strange behaviour in the retrievals (such as bad fitting residuals). The array overflows caused a minimum in the retrieved N_2O_5 VMR profile near 30 km, which became evident during the validation process. Hence, a new set of retrievals was performed for N_2O_5 using software with improved memory management to avoid the array overflows. This new data product has been provided as an update to version 2.2. The original v2.2 N_2O_5 data should not be used. The median N_2O_5 fitting errors, again examined for the group of ACE-FTS profiles as used for the MLS comparisons, are ~15% at 15 km and 40 km and below 5% from 20 to 35 km.

3 Validation approach

The ACE-FTS dataset used for these comparisons extends from 21 February 2004 (the start of the ACE Science Operations phase) through to 22 May 2007. The coincidence criteria were determined for each correlative dataset in consultation with the teams involved, while striving for consistency insofar as possible. The location of each ACE occultation is defined as the latitude, longitude and time of the 30-km tangent point (calculated geometrically). This value was used in searching for coincidences.

Coincidence criteria used for the satellite comparisons were between ±6 and ±12 h and between 300 and 800 km. Narrower criteria were chosen for MIPAS data products, for which correlative data was only available for a two-month period in early spring 2004 for northern mid- and high-latitudes. For the balloon and aircraft measurements, profiles obtained within ±26 h and 500 km of ACE-FTS were used. Finally, for the ground-based FTIRs, with some exceptions described in Sect. 6, the criteria were chosen as

ACPD
8, 2429–2512, 2008

±24 h and 1000 km to provide a reasonable number of coincidences. The correlative datasets, temporal and spatial coincidence criteria, and number of coincidences are summarized in Table 1 for the satellite and airborne instruments. Table 2 gives information on the FTIR locations and instruments used.

Differences in vertical resolution can influence comparisons, so these have been taken into account in this study. All the satellite instruments and the FIRS-2 balloon instrument have vertical resolutions that are similar to those of ACE-FTS. In these cases, no smoothing was applied to the data and the correlative profiles were linearly interpolated onto the 1-km ACE-FTS altitude grid.

For instruments with lower vertical resolution than ACE-FTS (the aircraft-based ASUR instrument and all ground-based FTIRs) the ACE-FTS profiles were degraded using the averaging kernel matrix and the a priori profile of the comparison instrument (Rodgers and Connor, 2003). Partial columns were calculated from all FTIR and coincident smoothed ACE-FTS profiles and used in the comparisons. The balloon-borne SPIRALE VMR profile was obtained at significantly higher vertical resolution than ACE-FTS, and so was convolved with triangular functions having full width at the base equal to 3 km and centered at the tangent height of each occultation. This approach simulates the smoothing effect of the 3–4 km ACE-FTS resolution, as discussed by Dupuy et al. (2007). The resulting smoothed profiles were interpolated onto the 1-km ACE-FTS grid. Co-located pairs of VMR profiles from ACE-FTS and each validation experiment (referred to as VAL in text and figures below) were identified using the appropriate temporal and spatial coincidence criteria. Then the following procedure was applied to the vertical profile measurements used in this assessment, with some modifications for the individual balloon-borne profile comparisons and the FTIR partial column comparisons (see Sects. 5 and 6 for details).

(a) Calculate the mean profile of the ensemble for ACE-FTS and the mean profile for VAL, along with the standard deviations on each of these two profiles. These mean profiles are plotted as solid lines, with $\pm 1\sigma$ as dashed lines, in panel (a) of the comparison figures discussed below. The standard error on the mean, also known as the

uncertainty in the mean, is calculated as $\sigma(z)/\sqrt{N(z)}$, where $N(z)$ is the number of points used to calculate the mean at a particular altitude, and is included as error bars on the lines in panel (a). Note: in some cases, these error bars, as well as those in panels (b) and (c) (see below) may be small and difficult to distinguish. (b) Calculate the profile of the mean absolute difference, ACE-FTS−VAL, and the standard deviation in the distribution of this mean difference (Note that the term absolute, as used in this work, refers to differences between the compared values and not to absolute values in the mathematical sense). To do this, the differences are first calculated for each pair of profiles at each altitude, and then averaged to obtain the mean absolute difference at altitude z:

$$\Delta_{\text{abs}}(z) = \frac{1}{N(z)} \sum_{i=1}^{N(z)} [\text{ACE}_i(z) - \text{VAL}_i(z)] \tag{2}$$

where $N(z)$ is the number of coincidences at z, $\text{ACE}_i(z)$ is the ACE-FTS VMR at z for the i^{th} coincident pair, and $\text{VAL}_i(z)$ is the corresponding VMR for the validation instrument. This mean absolute difference is plotted as a solid line in panel (b) of the comparison figures below, with $\pm 1\sigma$ as dashed lines. Error bars are also included in these figures. For the statistical comparisons involving multiple coincidence pairs (SMR, MLS, MIPAS, ASUR), these error bars again represent the uncertainty in the mean. For single profile comparisons (SPIRALE, FIRS-2), these error bars represent the combined random error, computed as the root-sum-square error of the ACE-FTS fitting error and the error for VAL. (c) Calculate the profile of the mean relative difference, as a percentage, defined using:

$$\Delta_{\text{rel}}(z) = 100\% \times \frac{1}{N(z)} \sum_{i=1}^{N(z)} \frac{[\text{ACE}_i(z) - \text{VAL}_i(z)]}{[\text{ACE}_i(z) + \text{VAL}_i(z)]/2}$$

$$= 100\% \times \frac{1}{N(z)} \sum_{i=1}^{N(z)} \frac{[\mathrm{ACE}_i(z) - \mathrm{VAL}_i(z)]}{\mathrm{MEAN}_i(z)} \quad (3)$$

where $\mathrm{MEAN}_i(z)$ is the mean of the two coincident profiles at z for the i^{th} coincident pair. Panel (c) of the comparison figures presents the mean relative difference as a solid blue line, along with the relative standard deviation as dashed lines, and the relative uncertainty in the mean as errors. Equation (3) gives the same weight to ratios with extremely small denominators, which contain, in relative terms more noise, thus overestimating the relative differences for these cases (von Clarmann, 2006). Therefore, we have calculated additionally the relative deviation from the mean using:

$$\begin{aligned}
\Delta_{\mathrm{mean}}(z) &= 100\% \times \frac{\frac{1}{N(z)} \sum_{i=1}^{N(z)} [\mathrm{ACE}_i(z) - \mathrm{VAL}_i(z)]}{\frac{1}{N(z)} \sum_{i=1}^{N(z)} [\mathrm{ACE}_i(z) + \mathrm{VAL}_i(z)]/2} \\
&= 100\% \times \frac{1}{N(z)} \sum_{i=1}^{N(z)} \frac{[\mathrm{ACE}_i(z) - \mathrm{VAL}_i(z)]}{\mathrm{MEAN}(z)} \\
&= 100\% \times \frac{\Delta_{\mathrm{abs}}(z)}{\mathrm{MEAN}(z)} \quad (4)
\end{aligned}$$

The relative deviation is added as a solid cyan line with its standard deviation as a dashed cyan line, in panel (c) for the $ClONO_2$ and N_2O_5 comparisons, where small VMRs at the lowest and highest altitude levels lead to overestimated relative differences. (d) Calculate the relative standard deviations on each of the ACE-FTS and VAL mean profiles calculated in step (a) for the statistical comparisons. For single profile comparisons, the relative values of the ACE-FTS fitting error and the error for VAL are determined instead. These results are plotted in panel (d) of the comparison figures, with the number of coincident pairs given as a function of altitude on the right-hand y-axis for the statistical comparisons.

4 Satellite measurements

4.1 Odin-SMR: HNO_3

The Odin satellite was launched in February 2001 into a near-polar, sun-synchronous, 600-km altitude orbit with an 18:00 ascending node (Murtagh et al., 2002). The Sub-millimetre Radiometer (SMR) observes limb thermal emission from HNO_3 on roughly two measurement days per week using an auto-correlator spectrometer centered at 544.6 GHz. Operational Level 2 HNO_3 retrievals are produced by the Chalmers University of Technology (Göteborg, Sweden).

Here we use Chalmers v.2.0 HNO_3 profiles, which have a horizontal resolution of ~300–600 km, vertical resolution of 1.5–2 km, and single-scan precision better than 1.0 ppbv over the range 18 to 45 km (Urban et al., 2006, 2007). The estimated total systematic error is less than 0.7 ppbv throughout the vertical range (Urban et al., 2005, 2006). The ACE-FTS–SMR coincidence criteria employed were ±12 h and 500 km. Whenever multiple SMR measurements were found to be coincident with the same ACE-FTS occultation, the SMR observation closest in distance was used. From these coincident measurements between February 2004 and November 2006 any SMR scan with a data quality flag value not equal to 0 was discarded. Furthermore, pairs of coincident data points were removed when either the ACE-FTS relative error exceeded 100% or the SMR response was below 0.75 (indicating that a priori information contributed significantly to the retrieved value) (Urban et al., 2005; Barret et al., 2006). The number of remaining coincident pairs used in the comparisons are shown along the right hand axis in Fig. 2d. The decrease in the number of comparison pairs below 20 km is due to declining SMR response, while above 32 km it is due to an increasing relative error in the ACE-FTS HNO_3 retrievals.

Figure 2 shows the statistical comparisons of all coincident profiles. Seasonal and/or latitude-limited comparisons were found to be of similar character, as were comparisons separated into SMR daytime or nighttime groups (not shown). The SMR and ACE-FTS mean profiles (Fig. 2a) have the same general shape, but detect the HNO_3

ACPD
8, 2429–2512, 2008

maximum at different altitudes. The ACE-FTS HNO_3 maximum (~23 km) is at a higher altitude than the SMR maximum (~21 km). The magnitude of the standard deviation of the means in Fig. 2 suggests that the SMR data is considerably noisier particularly above 30 km. The ACE-FTS VMR is typically 1.7 parts per billion by volume (ppbv), and at most 2.7 ppbv, smaller than SMR in the lower stratosphere (18–27 km). Above 27 km, the ACE-FTS VMR is typically 0.5 ppbv (at most 0.7 ppbv) larger than SMR (Fig. 2b). The mean relative difference (Fig. 2c) exceeds −100% at 17.5 km. This negative difference decreases towards higher altitudes and changes to positive relative differences at 27 km. Typically, it is ~15% (31%, at most) between 27 and 35 km.

This behaviour suggests an altitude shift between the two instruments, as was observed in MIPAS IMK-IAA – SMR HNO_3 comparisons by Wang et al. (2007b). Wang et al. (2007b) suggested an altitude shift of 1.5 km which is consistent with that found in MLS–SMR comparisons (Santee et al., 2007). To test this, an altitude shift of +1.5 km was applied to all SMR profiles. The shifted SMR profile and the comparison with the ACE-FTS are also shown in Fig. 2. For the shifted SMR mean profile, the HNO_3 maximum is at the same altitude as seen by ACE-FTS, around 23 km. That seems to confirm the existence and the size of the altitude shift as seen by the aforementioned satellite comparisons. Santee et al. (2007) suggested that it might be caused by systematic errors in the SMR 544.6 GHz pressure/temperature and pointing retrievals. The ACE-FTS HNO_3 VMRs are still up as much as 20% smaller than the shifted SMR values between 18 and 35 km, corresponding to a mean negative bias of -1 ppbv and a maximum negative bias of −1.9 ppbv at 25 km. These values are similar to the differences between MIPAS IMK-IAA and the altitude-shifted SMR as seen by Wang et al. (2007b), who concluded that other error sources (spectroscopy, calibration) may also contribute to the disagreement.

Although the SMR data display greater scatter, the latitudinal structure is very consistent with the ACE-FTS data, as seen in Fig. 3, including decreased HNO_3 values in the southern polar latitudes, where denitrification tends to occur. Individual points are plotted as a function of latitude for September, October, and November 2004–2006 at

altitudes between 18 and 22 km for both ACE-FTS and SMR. The 1.5-km altitude shift has been applied to the SMR data used in the plot.

4.2 Aura-MLS: HNO_3

The Microwave Limb Sounder (MLS) was launched on the Aura satellite in July 2004. It is in a sun-synchronous orbit at an altitude of 705 km and an inclination of 98°, with the ascending node crossing the equator at 13:45 (local time) (Waters et al., 2006). Global measurements are obtained daily from 82° S to 82° N, with 240 scans per orbit. Like SMR, MLS measures atmospheric thermal emission in the limb. Seven radiometers are used to provide coverage of five spectral regions between 118 GHz and 2.5 THz. The standard MLS HNO_3 product is derived from the 240 GHz retrievals at and below (i.e., at pressures equal to or larger than) 10 hPa and from the 190 GHz retrievals above that level (Livesey et al., 2007). The retrieval is performed on a pressure grid with six levels per decade for pressures greater than 0.1 hPa and three levels per decade for pressures less than 0.1 hPa using the optimal estimation approach described by Livesey et al. (2006). The vertical resolution for the HNO_3 VMR profiles is 3.5–5 km, the along-track horizontal resolution is 300–500 km. Validation of the MLS v2.2 HNO_3 data product is described by Santee et al. (2007). The precision of the individual MLS v2.2 HNO_3 profiles is estimated to be ~0.6–0.7 ppbv, and the recommended pressure range for the use for scientific studies is 215–3.2 hPa (Livesey et al., 2007).

Santee et al. (2007) compared ACE-FTS v2.2 HNO_3 with MLS HNO_3 measurements. They found that ACE-FTS values are slightly larger than those from MLS but agree to within 0.5–1 ppbv on average, corresponding to ~10% between 19 and 30 km and to ~30% above. Below 19 km, the differences increased and exceeded 50% where average VMRs are very low.

For their study, Santee et al. (2007) used an initial subset of the MLS v2.2 reprocessed data. Coincidence criteria, defined as ±12 h, ±1° latitude, and ±8° longitude, provided 1010 coincidences for the comparisons with ACE-FTS HNO_3, encompassing all seasons. The present study thus extends the analyses of Santee et al. (2007), us-

ing data from 15 September 2004 through 22 May 2007, which includes 7178 pairs obtained using the same coincidence criteria. Figure 4 shows the statistical comparisons of all coincident ACE-FTS and MLS profiles. In agreement with the results of Santee et al. (2007), the ACE-FTS mean HNO_3 profile is consistently ~0.6 ppbv (maximum difference = 0.8 ppbv) larger than that of MLS. The mean relative differences of the global comparisons are less than 23% between 18 and 32 km, and reach a minimum of 7% at approximately 25 km. The relative differences reach maxima of ~30% at the top and bottom of the altitude range where the mean HNO_3 profile reaches its lowest values.

The statistical comparison is divided into five latitude bands in Fig. 5. The relative differences in the northern (Fig. 5, part 1, middle row) and southern (Fig. 5, part 2, top row) midlatitude bands are ~10% between 18 and 27 km, within 20% between 28 and 32 km, and increase to 35% above 32 km. At the lowest altitudes, 15–18 km, the mean relative difference reaches 50% for the northern mid-latitudes and exceeds 100% for the southern mid-latitudes. The HNO_3 profiles in the polar latitude bands (Fig. 5, part 1, top row and part 2, bottom row) agree to within 20% between 18 and 30 km and within 40% above and below this range. The standard deviation of the mean relative difference increases dramatically below 22 km for the 60°–90° S latitude band, indicating a large spread in the differences between the individual comparisons. No distinction was made between measurements in and outside the polar vortex. Therefore, the large variance is a result of large spatial gradients in HNO_3 across the polar vortex edge at these altitudes in winter when denitrification drastically reduces the HNO_3 VMRs inside the vortex (Santee et al., 2004). Due to the typically lower HNO_3 values in the tropical regions, the mean relative differences are largest in the 30° S–30° N latitude band (Fig. 5, part 1, bottom row) varying from −10% to +40% between 20 and 35 km and exceeding 100% below. The absolute differences between 16 and 21 km are very small, within ±0.09 ppbv.

4.3 Envisat-MIPAS: HNO_3, $ClONO_2$, and N_2O_5

The Michelson Interferometer for Passive Atmospheric Sounding (MIPAS) is an infrared limb-sounding Fourier transform interferometer on board the Envisat satellite, launched in March 2002 (Fischer et al., 2007). MIPAS provides nearly pole-to-pole coverage (87° S–89° N) every day, measuring continuously around an orbit in both day and night. It acquires emission spectra over the range 685–2410 cm^{-1} (14.5–4.1 μm), which includes the vibration-rotation bands of many molecules of interest. From July 2002 until March 2004, MIPAS was operated at full spectral resolution (0.025 cm^{-1}) with a nominal limb-scanning sequence of 17 steps from 68–6 km with 3 km tangent height spacing in the troposphere and stratosphere, generating complete profiles spaced approximately every 500 km along the orbit. In March 2004, operations were suspended following problems with the interferometer slide mechanism. Operations were resumed in January 2005 with a 35% duty cycle and reduced spectral resolution (0.0625 cm^{-1}).

The European Space Agency (ESA) produces profiles of pressure, temperature, and six key species, among them HNO_3. The algorithm used for the Level 2 analysis is described in detail by Ridolfi et al. (2000), Carli et al. (2004), and Raspollini et al. (2006). Complementary to the ESA operational data products, several different off-line data processors are in use for science-oriented analysis of the MIPAS data (von Clarmann et al., 2003). The MIPAS IMK-IAA data processor was developed at the IMK, Germany, including a component to allow non-local thermodynamic equilibrium treatment from the IAA, Spain (von Clarmann et al., 2003). HNO_3, $ClONO_2$, and N_2O_5 are three of the trace gases retrieved with the MIPAS IMK-IAA processor and are available at http://www-imk.fzk.de/asf/ame/envisat-data/.

4.3.1 HNO_3

MIPAS HNO_3 profiles, retrieved with the ESA (v4.61/4.62) operational and IMK-IAA (v7/8) science data processors, were compared to ACE-FTS HNO_3 profiles by Wang et al. (2007a) and Wang et al. (2007b), respectively. Coincidence criteria for the

HNO_3 comparisons were defined in both papers as ±9 h, 800 km, and a maximum potential vorticity (PV) difference of $\pm 3 \times 10^{-6}$ K m^2 kg^{-1} s^{-1} at 475 K potential temperature. Wang et al. (2007a) and Wang et al. (2007b) compared about 600 daytime and nighttime MIPAS profiles to about 350 ACE-FTS coincident profiles, separated into two different latitude bands: 30–60° and 60–90°, resulting in a mean distance of 280±151 km and a mean time difference of 7.1±8.4 h. The consistency between both MIPAS HNO_3 products (ESA and IMK-IAA) and ACE-FTS HNO_3 was found to be very good. The mean differences were between ±0.1 and −0.5 ppbv for the ACE-FTS versus MIPAS ESA data product comparisons (Wang et al., 2007a) and between ±0.1 and −0.7 ppbv for the ACE-FTS versus MIPAS IMK-IAA data product comparisons (Wang et al., 2007b). That corresponds to relative differences between ±5 and ±10% for altitudes between 10 and 30 km and between ±10 and ±15% for altitudes above (up to 35 km) (Wang et al., 2007a,b).

In both papers, data were analysed for the period 9 February to 25 March 2004, including data from the ACE satellite commissioning period which continued until 21 February 2004. We recalculated the comparisons between ACE-FTS sunset observations and MIPAS for the period 21 February to 25 March 2004 using only data from the ACE Science Operations period. Figures 6 and 7 show the results of these revised comparisons.

For the comparison with the MIPAS ESA data used in this work (v4.62), we narrowed the coincidence criteria to ±6 h and 300 km, resulting in 138 coincident profiles, shown in Fig. 6. The mean difference between ACE-FTS and MIPAS ESA HNO_3 is typically −0.1 ppbv and varies between −0.71 ppbv at 27.5 km and +0.33 ppbv at 30.5 km. That corresponds to typically ±2% between 10 and 27 km and to ±9% between 27 and 36 km. A maximum relative difference of −25% is obtained for the highest comparison altitude of 36.5 km.

The comparison between the ACE-FTS and MIPAS (IMK-IAA v8) HNO_3 products was calculated using the same coincidence criteria as defined by Wang et al. (2007b) and is shown in Fig. 7. Between 10 and 31 km, ACE-FTS is typically is 0.2 ppbv smaller

ACPD
8, 2429–2512, 2008

than MIPAS IMK-IAA HNO_3. Mean relative differences are mainly within ±2% and do not exceed ±9%. Above 31 km, ACE-FTS reports larger values than MIPAS. The mean relative differences are between 5 and 17%.

4.3.2 $ClONO_2$

MIPAS $ClONO_2$ VMR data are retrieved with the IMK-IAA scientific data processor using the microwindow centered at 780.2 cm^{-1}. Höpfner et al. (2007) compared $ClONO_2$ profiles from MIPAS (IMK-IAA v10/11) with ACE-FTS $ClONO_2$ profiles for the period 9 February to 25 March 2004. Comparisons were carried out for the latitude bands 30–60° N and 60–90° N and separated for MIPAS daytime and nighttime measurements. Coincidence criteria used for the $ClONO_2$ comparisons were ±9 h, 800 km, and a maximum PV difference of $\pm 3 \times 10^{-6}$ K m^2 kg^{-1} s^{-1} at 475 K potential temperature. When combining all coincidences, the mean differences between ACE-FTS and MIPAS $ClONO_2$ were found to be less than 0.04 ppbv (<5%) up to altitudes of 27 km. At nearly all altitudes, ACE-FTS reported smaller VMR values than MIPAS. Above 27 km, the differences increased to around −0.15 ppbv (−30% at 34.5 km). In the altitude range between 15 and 19 km, slightly enhanced differences of up to −0.03 ppbv could be observed (Höpfner et al., 2007). The high-altitude bias was assumed to be photochemically induced. Therefore, Höpfner et al. (2007) used the KArlsruhe SImulation model of the Middle Atmosphere Chemical Transport Model (KASIMA CTM) (Kouker et al., 1999) to transform the MIPAS profiles to the time and location of ACE-FTS occultations. From a multi-annual run with a horizontal resolution of approximately $2.6 \times 2.6°$ (T42), a vertical resolution of 0.75 km from 7 to 22 km and an exponential increase above with a resolution of about 2 km in the upper stratosphere, and a model time step of 6 min, $ClONO_2$ profiles were interpolated to the time and position of the measurements of ACE-FTS and of MIPAS: $\boldsymbol{x}_{\mathrm{ACE}}^{\mathrm{CTM}}$ and $\boldsymbol{x}_{\mathrm{MIPAS}}^{\mathrm{CTM}}$. For the intercomparison, the original MIPAS profiles $\boldsymbol{x}_{\mathrm{MIPAS}}$ were transformed to the time and position of the ACE-FTS measurements by adding the relative difference between the two model results.

ACPD
8, 2429–2512, 2008

Relative differences were used to account for any problems with the absolute values of modeled NO_y. The expression used is:

$$x_{\mathrm{MIPAS}}^{\mathrm{CTMcorr}} = x_{\mathrm{MIPAS}} + \frac{x_{\mathrm{ACE}}^{\mathrm{CTM}} - x_{\mathrm{MIPAS}}^{\mathrm{CTM}}}{x_{\mathrm{MIPAS}}^{\mathrm{CTM}}} \times x_{\mathrm{MIPAS}}. \quad (5)$$

In the resulting comparison between ACE-FTS and the CTM-corrected MIPAS $ClONO_2$ VMRs, the maximum absolute differences were reduced and no systematic bias up to 27 km altitude was seen. At higher altitudes, however, the model overcompensated for the photochemically-induced bias and the corrected MIPAS $ClONO_2$ values were up to 0.1 ppbv smaller than those measured by ACE-FTS (Höpfner et al., 2007).

For this paper, we recalculated the comparison between ACE-FTS and MIPAS $ClONO_2$ using IMK-IAA v11 for the period 21 February to 25 March 2004, considering only the ACE-FTS data after the start of the ACE Science Operations period. The results of the comparisons, which do not change significantly the findings of Höpfner et al. (2007), are shown in Fig. 8. The ACE-FTS $ClONO_2$ values are smaller than the uncorrected MIPAS product for all altitudes. The mean relative differences are better than −7% between 16 and 27 km, and reach −30% at 34 km (Fig. 8, top row). The comparison between ACE-FTS and the CTM-corrected MIPAS $ClONO_2$ profiles shows no systematic difference between 16 and 27 km. Typically mean relative differences are within ±1%, reaching a maximum of −6% around 16–17 km. Above 27 km, ACE-FTS $ClONO_2$ is larger than the corrected MIPAS values with a maximum relative difference of 22% around 33 km (Fig. 8, bottom row), suggesting that the model is overcompensating as observed in the previous study.

As explained in Sect. 3, Eq. (3) overestimates the relative differences in the lowest altitude region, 13–16 km, when some denominators are extremely small. Therefore, profiles of the relative deviation of the mean, calculated with Eq. (4), are also included in Fig. 8. The relative deviation of the mean clearly shows that ACE-FTS is very consistent with MIPAS $ClONO_2$ also at lower altitudes, differing not more than −6% between

13 and 16 km.

4.3.3 N_2O_5

The retrieval method and characteristics of N_2O_5 profiles inverted from MIPAS observations have been described by Mengistu Tsidu et al. (2004). N_2O_5 is retrieved from its infrared emission in the ν_{12} band in the spectral range from 1239–1243 cm^{-1}. Spectroscopic data for N_2O_5 by Wagner and Birk (2003) were taken from the HITRAN 2004 database (Rothman et al., 2005). The vertical resolution, in the case of mid-latitude profiles, is about 4–6 km between 30 and 40 km and 6–8 km below 30 km and between 40 and 50 km. The measurement noise is between 5 and 30% in the altitude range of 20–40 km. The systematic errors are within 10–45% at 20–40 km and increase up to 75% outside this region.

Here we compare N_2O_5 profiles from ACE-FTS observations and MIPAS IMK-IAA v9 measurements from 21 February 2004 until 25 March 2004. For the comparisons, we again used as coincidence criteria a maximum time difference of ±9 h, a maximum tangent point difference of 800 km, and a maximum PV difference of $\pm 3\times10^{-6}$ $Km^2\,kg^{-1}\,s^{-1}$ at the 475 K potential temperature level.

In Fig. 9, we show separately the results of the comparisons between ACE-FTS and MIPAS IMK-IAA daytime (first row) and MIPAS IMK-IAA nighttime N_2O_5 profiles (third row). MIPAS measurements occur either in the late morning or early night, while the ACE-FTS observations used here are made during sunset. Thus, for comparison with nighttime MIPAS observations, the time difference (ACE-FTS–MIPAS) is −4 to −5 h, while in the case of MIPAS daytime measurements it is about +6 to +8 h.

At the altitude of the N_2O_5 VMR maximum (around 30 km), ACE-FTS VMRs are ∼0.5 ppbv (75%) smaller than MIPAS IMK-IAA daytime observations and ∼0.4 ppbv (70%) smaller than the MIPAS IMK-IAA nighttime observations. At altitudes below the VMR maximum, these differences decrease in absolute terms. In relative terms, however, largest differences appear at around 18 km and at the highest altitudes, just below 40 km.

To account for the diurnal cycle of N_2O_5 and the different local observation times of MIPAS and ACE-FTS, we have performed a correction using the KASIMA CTM (Kouker et al., 1999), as was done for $ClONO_2$. Rows 2 and 4 of Fig. 9 show results of the CTM-corrected comparisons for MIPAS IMK-IAA daytime and MIPAS IMK-IAA nighttime measurements, respectively. In both cases, the large differences at the VMR maximum are reduced by a factor of 2–4 and the difference profiles for daytime and nighttime comparisons have become more similar. In relative units, ACE-FTS N_2O_5 is now about ∼40% smaller than MIPAS IMK-IAA near the VMR maximum. Maximum absolute differences are −0.25 ppbv for daytime and −0.22 ppbv for nighttime measurements. Between 16 and 27 km, ACE-FTS VMRs typically differ by ±0.02 ppbv (maximum +0.04 ppbv) from the MIPAS CTM-corrected daytime VMRs and by −0.05 ppbv (maximum −0.09 ppbv) from the MIPAS CTM-corrected nighttime VMRs. Above the N_2O_5 VMR maximum at 30 km, the relative deviation of the mean is again a better measure of the agreement. ACE-FTS is ∼25% smaller than the CTM-corrected MIPAS N_2O_5 around 35 km.

To address the question of whether the remaining differences are caused by the MIPAS observations, we compared MIPAS IMK-IAA N_2O_5 results with coincident MIPAS-Balloon observations, for which no diurnal corrections are necessary. No systematic overestimation by MIPAS is seen: maximum differences at 30 km range from 0 to 0.1 ppbv with relative differences of 0–10% at mid-latitudes in September 2002 and up to 20% at high latitudes in March 2003 near the boundary of the polar vortex. Thus, we conclude that either there might be a low bias of ACE-FTS N_2O_5 relative to MIPAS IMK-IAA around 30 km, or, more probably, that the correction by using a CTM, which improved the comparison significantly, still contains some uncertainty.

5 Airborne measurements

5.1 ASUR on NASA DC-8: HNO_3

The Airborne SUbmillimeter wave Radiometer (ASUR) from the University of Bremen is a passive heterodyne receiver operating over a tunable frequency range from 604.3 to 662.3 GHz (von König et al., 2000). The microwave sensor houses two spectrometers, an Acousto Optical Spectrometer (AOS) and a Chirp Transform Spectrometer. Stratospheric measurements taken with the AOS are used for this validation analysis. The total bandwidth of the AOS is 1.5 GHz and its resolution is 1.27 MHz. The HNO_3 retrieval uses a rotational band around 606.8 GHz (Kleinböhl et al., 2003). The measurements are carried out aboard a high-altitude research plane (NASA DC-8) to avoid signal absorption by tropospheric water vapour. ASUR takes observations through the limb of the atmosphere at a constant solar zenith angle of 78°. Thermal emissions from the rotational states of the molecules are detected by the radiometer and the shape of the pressure-broadened lines can be related to the vertical distribution of the species. The measured spectra are integrated over 90 s to achieve a sufficient signal-noise-ratio. The horizontal resolution of the HNO_3 profile is ~20 km, which depends on the ground speed of the aircraft and the integration time. The vertical profiles are retrieved on a 2-km grid, using the optimal estimation method (Rodgers, 2000). The vertical resolution of the HNO_3 measurement is 6–10 km in the lower stratosphere and a retrieval is possible between 15 and 35 km. The precision of a typical measurement is 0.3 ppbv and the estimated accuracy is ~0.6 ppbv or 15%, whichever is higher (von König et al., 2000; Kleinböhl et al., 2003).

The ASUR HNO_3 measurements performed during the Polar Aura Validation Experiment (PAVE) (Kleinböhl et al., 2005) are compared to ACE-FTS HNO_3. As criteria for the intercomparison, ASUR measurements within 500 km and ±6 h of the satellite observations were chosen. This resulted in a total of 16 coincident measurements from five ASUR flights (24, 29, and 31 January 2005, and 2 and 7 February 2005). Since the observations were performed during the 2004–2005 winter, most coincident

measurements were found inside the polar vortex. For this, the vortex edge was estimated by applying the criterion of Nash et al. (1996) using the European Centre for Medium-Range Weather Forecasts (ECMWF) meteorological analysis. The ACE-FTS VMRs were convolved with the ASUR HNO_3 averaging kernels to account for the lower vertical resolution of the ASUR profiles.

Figure 10 shows the results from the comparison. The ACE-FTS VMRs are slightly larger in the lower stratosphere and smaller in the middle stratosphere than those VMRs from ASUR. The ACE-FTS–ASUR differences are up to 2.5 ppbv or 32% in the lower stratosphere (between 18 and 26 km) and are up to −0.3 ppbv or −6% in the middle stratosphere (28–36 km). The sign of these differences changes at 27.5 km.

5.2 SPIRALE balloon: HNO_3

SPIRALE (SPectroscopie Infra-Rouge d'Absorption par Lasers Embarqués) is a balloon-borne instrument operated by the Laboratoire de Physique et Chimie de l'Environnement (Centre National de la Recherche Scientifique – Université d'Orléans) and routinely used at all latitudes, in particular as part of recent European satellite validation campaigns for Odin and Envisat. SPIRALE performs simultaneous in situ measurements for about ten chemical species using six tunable lasers (Moreau et al., 2005). Measurements are done during the balloon ascent from about 10 to 35 km height, with a high frequency sampling (∼1 Hz), thus providing a vertical resolution of only a few meters. The diode lasers emit in the mid-infrared domain (from 3 to 8 µm) with beams injected into a 3.5-m-long multipass Heriott cell located under the gondola and largely exposed to ambient air. A total optical path length of 430.78 m is obtained by multiple reflections between the two cell mirrors. Species concentrations are retrieved from direct infrared absorption, by fitting experimental spectra with spectra calculated using the HITRAN 2004 database (Rothman et al., 2005). The species concentration can be converted into VMR using the on-board pressure and temperature measurements. Specifically, the ro-vibrational lines in the microwindow 1701.5–1701.8 cm^{-1} were used for HNO_3 (Moreau et al., 2005).

The global uncertainties for the VMRs have been assessed by taking into account the random errors and the systematic errors, and combining them as the square root of their quadratic sum. The two important sources of random errors are the fluctuations of the laser background emission signal and the signal-to-noise ratio. The laser line width and the non-linearity of the detector contribute to the systematic errors. The resulting global uncertainty is estimated to be 25% below 17 km, and 20% above. With respect to the above errors, systematic errors in the spectroscopic data (essentially molecular line strength and pressure broadening coefficients) are considered to be negligible.

The SPIRALE measurements occurred on 20 January 2006 between 17:46 UT and 19:47 UT, with vertical profiles obtained between 13.7 and 27.2 km altitude. The measurement position remained relatively constant, with the balloon mean location of 67.6±0.2° N and 21.55±0.20° E. The comparison is made with ACE-FTS sunrise occultation sr13151 on 21 January 2006, 08:00 UT, located at 64.28° N and 21.56° E, 413 km away from the SPIRALE location and 13 h later. Using the MIMOSA (Modélisation Isentrope du transport Mésoéchelle de l'Ozone Stratosphérique par Advection) contour advection model (Hauchecorne et al., 2002). PV maps in the region of both measurements have been calculated each hour between 17:00 UT on 20 January and 08:00 UT on 21 January on isentropic surfaces, every 50 K from 350 K to 800 K (corresponding to 13–30 km height). From these PV fields, it can be deduced that SPIRALE and ACE-FTS vertical profiles were located in similar air masses in the well-established polar vortex for the whole range of altitudes sounded by SPIRALE. The dynamical situation was very stable with PV agreement better than 10%. So the geophysical situation is suitable for direct comparisons. As mentioned in Sect. 3, SPIRALE data were smoothed with a triangular weighting function of 3 km at the base (corresponding to ACE-FTS resolution). Consequently, the bottom and the top of the SPIRALE profile have been truncated by 1.5 km. The resulting profile was subsequently interpolated onto the 1-km ACE-FTS grid. Possible diurnal variations due to the different times of the day of the measurements (SPIRALE flew at night and ACE-FTS measurements were at sunrise) have been examined with a photochemical box model (McLinden et al., 2000). It

ACPD
8, 2429–2512, 2008

appears that the diurnal variations in HNO_3 were negligible.

Figure 11 shows that the ACE-FTS HNO_3 profile is systematically larger than the SPIRALE profile. Between 15 and 23 km, ACE-FTS and SPIRALE agree to within 45% and within 13% between 23 and 26 km. The low HNO_3 values observed by SPIRALE in the 20.7–22 km layer are probably due to the polar stratospheric cloud (PSC) that SPIRALE encountered from 19.3 to 20.7 km, which was detected by an aerosol counter aboard the gondola. Using HYSPLIT (Draxler and Hess, 1998a,b) backward trajectories above 20.7 km, it appears that the temperature encountered along the trajectories was close to the nitric acid trihydrate equilibrium temperature during the two days before the measurements. The low temperatures encountered by the air parcel probably allowed formation of PSC particles with large size (greater than 1 µm), leading to a denitrified layer. By the time the SPIRALE measurements were made, the PSC had sedimented.

5.3 FIRS-2 balloon: HNO_3, $ClONO_2$, N_2O_5

The balloon-borne Fourier transform infrared spectrometer FIRS-2 (Far-InfraRed Spectrometer-2) was designed and built at the Smithsonian Astrophysical Observatory. It has contributed to previous satellite validation efforts (e.g., Jucks et al., 2002; Nakajima et al., 2002; Canty et al., 2006). FIRS-2 detects atmospheric thermal emission in limb-viewing mode from approximately 7 to 120 μm (~80–1350 cm^{-1}) at a spectral resolution of 0.004 cm^{-1} (Johnson et al., 1995). Vertical profiles of about 30 trace gases are retrieved from the float alitude (typically 38 km) down to the tropopause using a nonlinear Levenberg-Marquardt least-squares algorithm, with pressure and temperature profiles dervied from the 15 μm band of CO_2. HNO_3 is retrieved from the ν_9 band between 440 and 470 cm^{-1}. The retrievals from the ν_5 and $2\nu_9$ bands, made with the HITRAN 2004 dataset differ systematically by 2%. $ClONO_2$ is retrieved jointly with the ν_5 band at 560 cm^{-1} and the q-branch of the 720 cm^{-1} band. N_2O_5 is retrieved from the band between 710 and 770 cm^{-1}. However, the signal-to-noise ratio is not very good

ACPD
8, 2429–2512, 2008

for this particular retrieval. Uncertainty estimates for FIRS-2 contain random retrieval error from spectral noise and systematic compontents from errors in atmospheric temperature and pointing angle (Johnson et al., 1995; Jucks et al., 2002). We compare ACE-FTS HNO_3, $ClONO_2$, and N_2O_5 profiles with the data obtained during a FIRS-2 balloon flight from Esrange, Sweden on 24 January 2007 at 10:11 UT. The average location of the flight was 67.27° N and 27.29° E, with some smearing of the longitude footprint as FIRS-2 was observing to the east. The data were recorded before local solar noon with a solar zenith angle of 86.6°. The float altitude was just under 28 km, limiting the maximum measurement altitude to 31 km. The closest ACE-FTS occultation was sr18561, obtained on 23 January 2007, at 08:25 UT (64.70° N, 15.02° E), placing it 26 h earlier and 481 km away from the location of the balloon flight. The FIRS-2 trace gas profiles are reported on a 1-km grid and were interpolated onto the ACE-FTS 1-km grid.

Figure 12 shows the comparisons of the VMR profiles of HNO_3 (top row), $ClONO_2$ (middle row), and N_2O_5 (bottom row) measured by FIRS-2 and ACE-FTS. Scaled (Dunkerton and Delisi, 1986; Manney et al., 1994) PV values for the times and locations of both measurements indicate that both instruments measured airmasses inside the polar vortex. At the time of the FIRS-2 flight, PSCs could be observed from the ground and the scattering of the upwelling radiation in the spectra indicated that the balloon gondola passed through a PSC during the flight. Also, there is a slight enhancement in the ACE-IMAGER extinction data at 20 km for this occultation, which may have been caused by the presence of PSCs.

5.3.1 HNO_3

The ACE-FTS HNO_3 VMR profile shows values up to 3 ppbv smaller than the FIRS-2 VMR from 15 to 18 km (−25%) and from 26 to 31 km (−55%). In the altitude range between 19 and 25 km, ACE-FTS measured values that were up to 3 ppbv larger than FIRS-2. Relative differences in this altitude range reach at most 50% at 20 km. The low FIRS-2 HNO_3 values between 19 and 25 km are very likely due to a denitrified

ACPD
8, 2429–2512, 2008

layer caused by sedimenting PSC particles. That is often accompanied by enhanced HNO_3 values at the altitudes below, where the sedimenting particles reach warmer air, sublimate and form layers with higher concentration of nitrogen oxides. This is a possible explanation for the larger HNO_3 VMRs between 15 and 18 km detected by FIRS-2. Although the ACE-FTS occultation may also have detected a PSC near 20 km, the HNO_3 VMR shows only a small decrease at this level. Maps of the HNO_3 distribution obtained from MLS data for 24 January 2007 at the 490 and 520 K potential temperature levels (approximately 20.5 and 21.5 km for the ACE-FTS profile) show that the comparison measurements were located at the edge of a fairly extensive region of PSCs indicated by strong HNO_3 gradients. The ACE-FTS measurements were made closer to the edge of this region than FIRS-2, consistent with the differences seen in the HNO_3 VMRs of the two profiles we compared.

5.3.2 $ClONO_2$

For altitudes above 25 km, ACE-FTS measures up to 0.8 ppbv less $ClONO_2$ than FIRS-2. Due to the large FIRS-2 uncertainties at these altitudes, the differences are within the combined random errors. Below 25 km, the ACE-FTS VMR profile shows a decrease in $ClONO_2$, whereas FIRS-2 measures significantly enhanced $ClONO_2$ values between 20 and 25 km, thus resulting in a disagreement of up to −2.8 ppbv or −150% between ACE-FTS and FIRS-2 in this altitude range. At this time, these differences are unexplained and are under investigation. The large FIRS-2 $ClONO_2$ VMRs within this altitude range could be due to retrieval problems or could indicate a real feature. Below 18 km, the FIRS-2 $ClONO_2$ values are slightly negative and fractional uncertainties exceed 200%, whereas ACE-FTS values are ∼0.15 ppbv. Due to the negative FIRS-2 values, the resulting relative differences exceed 300%.

5.3.3 N_2O_5

From 16 to 26 km, FIRS-2 N_2O_5 VMRs are equal to zero within the statistical variability of the measurements. Between 27 and 31 km, FIRS-2 measured an N_2O_5 VMR of ~1.5 ppbv. A low signal-to-noise ratio for this particular retrieval is reflected in the extremely high fractional uncertainties, as high as 10 000% between 16 and 23 km and ~50% at about 29 km. The ACE-FTS N_2O_5 VMR increases gradually from ±0.01 ppbv between 16 and 19 km to 1.2 ppbv at 30 km. Given the size of the FIRS-2 uncertainties below 27 km, a meaningful comparison is only possible for higher altitudes. ACE-FTS VMRs are up to 0.6 ppbv smaller than FIRS-2 VMR between 27 and 31 km and are within the combined error bars.

6 Ground-based measurements: HNO_3 and $ClONO_2$

ACE-FTS HNO_3 and $ClONO_2$ measurements were also compared with partial columns retrieved from solar absorption spectra recorded by ground-based Fourier transform infrared spectrometers. All of the FTIR instruments are located at NDACC stations, except the Poker Flat FTIR which is a NDACC candidate instrument, currently waiting for its certification.

Table 2 lists the stations, their locations, and further details regarding the instrument type, the spectral resolution, the retrieval code and the microwindows used to retrieve HNO_3 and $ClONO_2$. The references in Table 2 provide more information about the instruments, the retrieval techniques and the measurements made at each station. The participating sites span latitudes from 77.8° S to 76.5° N. The geographical locations of these sites are shown in Fig. 13.

The FTIR data were analyzed using either the SFIT2 retrieval code (Pougatchev and Rinsland, 1995; Pougatchev et al., 1995; Rinsland et al., 1998) or PROFFIT92 (Hase, 2000). Hase et al. (2004) showed that VMR profiles and total columns retrieved using these two codes are in very good agreement (total columns of HNO_3 agree

ACPD
8, 2429–2512, 2008

within 1%). Considering the slightly different handling of spectroscopic data for the $ClONO_2$ retrieval, one can expect that PROFFIT92 and SFIT2 retrieved $ClONO_2$ agree within ±2%. Both algorithms employ the optimal estimation method (Rodgers, 2000) to retrieve vertical profiles from a statistical weighting between a priori information and the high-resolution spectral measurements. Averaging kernels calculated as part of this analysis quantify the information content of the retrievals, and can be convolved with the ACE-FTS profiles, which have higher vertical resolution. The information required for the retrievals, such as a priori profiles and covariances, treatment of instrument lineshape, and atmospheric temperature and pressure are optimized for each site as appropriate for the local conditions.

The coincidence criteria used for the FTIR comparisons are ±24 h and 1000 km, with three exceptions. For the high-latitude stations Kiruna and Thule, tighter criteria of ±12 h and 500 km were used, in order to minimize the influence of the polar vortex. Note that for Poker Flat and Arrival Heights, these tighter criteria would have reduced the number of coincidences too much. Therefore, the original criteria (±24 h, 1000 km) were kept for these two high latitudes stations. For Reunion Island, the criteria were ±24 h, ±10 degrees latitude, and ±15 degrees longitude, resulting in a maximum spatial difference of 1211 km. These relatively relaxed criteria were necessary to obtain a reasonable number of ACE overpasses for each station (between 5 and 29). In cases where several ACE-FTS occultations met the coincidence criteria for one FTIR measurement at a site, only the closest ACE occultation (optimized for temporal and spatial differences) was used.

The comparisons include coincident measurements from March 2004 through October 2006. For each station, the ACE-FTS profiles were interpolated onto the FTIR retrieval grid and extended below the lowest retrieved altitude using the FTIR a priori VMR values. This combined profile was smoothed using the FTIR averaging kernels and a priori profile, as described in Sect. 3, to minimize the smoothing error (Rodgers and Connor, 2003). Atmospheric density profiles were calculated based on the pressure and temperature profiles used in the FTIR retrievals. These FTIR density profiles

ACPD
8, 2429–2512, 2008

were used to calculate partial columns from the smoothed ACE-FTS profiles and the retrieved FTIR profiles, except for Jungfraujoch where the ACE-FTS partial columns were calculated using the ACE-FTS density profiles.

The altitude ranges of the partial columns were determined separately for each station and species. Each altitude range is limited to the altitude levels that fulfill two criteria: (1) ACE-FTS retrievals have to exist, and (2) the sensitivity of the FTIR measurements has to be 0.5 or greater, indicating that the measurement contributes at least 50% to the retrieved profile. The latter can be determined from the FTIR a priori information and the averaging kernel matrix (Vigouroux et al., 2007). The chosen altitude ranges are listed in Tables 3 and 4.

6.1 HNO_3

For the retrievals of HNO_3, all FTIR sites used spectroscopic data from the HITRAN 2004 database (Rothman et al., 2005). All participating sites used microwindows in the region 860–875 cm^{-1} as listed in Table 2. The Degrees of Freedom of Signal (DOFS) of the FTIR partial columns (equal to the trace of the averaging kernel matrix) are between 1 and 2, thus indicating there is enough independent information for a partial column.

The time series of the HNO_3 partial column comparisons are shown for all stations in Fig. 14, along with the relative differences as a percentage of the FTIR partial columns. The agreement between ACE-FTS and the FTIRs is typically ±20%, and does not exceed ±50% except for two cases measured at Arrival Heights, where the two ACE-FTS partial columns differ by ±150% from the four coincident FTIR partial columns. Table 3 summarizes these results, listing the mean relative differences (mean of the N differences (ACE-FTS–FTIR)/FTIR), the standard deviations, and standard errors on the mean.

The largest relative differences (given with standard error), $-11.4\% \pm 8.7\%$ and $-12.6\% \pm 14.4\%$, are reported for the comparisons with the two high-latitude stations Poker Flat and Arrival Heights, respectively. Both stations include a large number

ACPD
8, 2429–2512, 2008

of measurements in the polar winter and spring, the period with the greatest vortex activity. The large standard deviation of 59.2% for Arrival Heights is caused by two ACE-FTS occultations showing one exceptionally high and the other exceptionally low partial column values, both occuring in the late austral winter. Neglecting all winter and spring measurements for Arrival Heights improves the agreement between ACE-FTS and FTIR to 3.8% and decreases significantly the standard deviation on the mean difference to 20.4%. We suggest that the larger differences reported at these two stations are caused by the higher variability in the polar areas. That is supported by the comparison results of the two other polar stations, Thule and Kiruna, for which tighter coincidence criteria were applied. They show a positive bias of ~2.5% which is well within the mean relative differences of ±6% reported for the low- and midlatitude stations. At five of the nine stations, the mean relative difference is negative, thus suggesting a small negative bias in the ACE-FTS HNO_3 partial columns relative to the FTIR measurements, which is consistent with a mean relative difference of −1.3% (25.9% standard deviation) calculated from all coincident FTIR comparisons. Figure 15 shows good correlation between ACE-FTS and the FTIR HNO_3 partial columns, with a correlation coefficient R=0.823. The line fitted to the data has slope of 0.88 and intercept of 0.11×10^{16} molecules cm^{-2}. No significant latitudinal dependence of the bias could be identified.

In similar work, FTIR HNO_3 partial columns were compared with MIPAS ESA partial columns by Vigouroux et al. (2007) and were updated by Wang et al. (2007a). Wang et al. (2007a) found a mean relative difference of ±2% with 1σ standard deviations between ±5.4% and 13.2% using coincidence criteria defined as 300 km and ±3 h.

6.2 $ClONO_2$

Coincident data for this comparison with ACE-FTS was available from four FTIR stations. All FTIR retrievals of $ClONO_2$ used spectroscopic data from the HITRAN 2004 database (Rothman et al., 2005) with supplements from Wagner and Birk (2003), using a two-microwindow approach similar to that described by Reisinger et al. (1995).

The time series of the $ClONO_2$ partial column comparisons are shown for all stations in Fig. 16, along with the relative differences as a percentage of the FTIR partial columns. The mean difference results are given in Table 4. All stations show a large 1σ standard deviation on the mean relative differences. For the polar stations, the inhomogeneous $ClONO_2$ distribution in Arctic stratospheric airmasses during periods of high vortex variability will contribute to this variation. However, there appears to be no systematic dependence of the mean relative differences or their standard deviations on latitude. The mean relative difference between ACE-FTS and the midlatitude Jungfraujoch station is $4.7\% \pm 4.2\%$ with a 1σ standard deviation of 16.3%, which is the lowest standard deviation obtained for the $ClONO_2$ comparisons. It should be noted that the Wollongong dataset has a DOFS of only 0.3, thus indicating that the partial column contains less than 1 independent piece of information, and that there is a contribution from the noise.

The scatter plot of the complete dataset (Fig. 17) shows a fair correlation between ACE-FTS and the FTIR $ClONO_2$ partial columns, with a correlation coefficient R=0.815. The line fitted to the data has slope 0.71, thus being significantly lower than 1, and intercept 0.36×10^{15} molecules cm^{-2}. A possible reason for this are the different line parameters used for the $ClONO_2$ retrievals. Most of the information in the ACE-FTS partial columns is coming from the microwindow centered at 1292.6 cm^{-1}, whereas the FTIRs used microwindows around ~780 cm^{-1} for their retrievals. This is a topic for further investigation.

Höpfner et al. (2007) compared MIPAS IMK-IAA $ClONO_2$ partial columns with ground-based FTIR data using tighter coincidence criteria of 800 km, ±8 h, and additionally, a maximum PV difference of $3 \cdot 10^{-6}$ Km^2 kg^{-1} s^{-1} at 475 K. Relative differences were found to be between −9.2% and 10%.

ACPD
8, 2429–2512, 2008

7 Conclusions

In this study, we have undertaken an assessment of the quality of HNO_3, $ClONO_2$, and N_2O_5 data (ACE-FTS v2.2, including the N_2O_5 update) prior to its public release. All three molecules belong to the group of 14 baseline species for the ACE mission. HNO_3 is retrieved using 12 microwindows between 867–1728.6 cm^{-1}, covering an altitude range from 5 to 37 km. The $ClONO_2$ retrieval employs two microwindows, centered at 780.15 cm^{-1} and 1292.6 cm^{-1}, and covers altitudes between 12 and 35 km. N_2O_5 is retrieved from two microwindows between 1210 and 1270 cm^{-1} at altitudes from 15 to 40 km. All VMR profiles have a vertical resolution of about 3–4 km.

7.1 HNO_3

ACE-FTS HNO_3 profiles from the first three years of the mission have been compared with coincident measurements made by the SMR, MLS, and MIPAS (ESA and IMK-IAA data products) satellite instruments, multiple aircraft flights of ASUR, and individual balloon flights of SPIRALE and FIRS-2. ACE-FTS HNO_3 partial columns have been compared with measurements by nine globally distributed ground-based FTIRs. In Fig. 18, the mean absolute differences and the mean relative differences for all of the statistical and indvidual vertical profile comparisons are shown together, while Table 5 provides a summary of the results of these comparisons.

The comparison of ACE-FTS HNO_3 with the four satellite data products shows an agreement between −1.9 ppbv and +0.8 ppbv (±25%). On average, ACE-FTS has a negative bias with a maximum value of −0.7 ppbv relative to MIPAS (both the ESA and the IMK-IAA data products) and a slightly larger positive bias with a maximum value of +0.8 ppbv relative to MLS. Relative mean differences with respect to MIPAS and MLS are within ±10% between 19 and 26 km, as seen in Fig. 18. An altitude shift of 1.5 km was applied to the SMR profiles based on the results of previous assessments. The magnitude of the altitude shift and the remaining relatively large negative bias of −1.9 ppbv around 25 km is consistent with results from other satellite comparisons

(Wang et al., 2007a,b; Santee et al., 2007). Statistical comparisons also involved a set of 16 coincident pairs of ACE-FTS and ASUR aircraft observations. Between 18 and 26 km ACE-FTS HNO_3 VMRs are up to 2.5 ppbv (32%) larger than ASUR. Between 26 and 36 km, the two instruments typically agree within ±0.2 ppbv (±3%) which is consistent with the satellite comparisons.

Comparisons were also made with individual profiles obtained from two balloon flights. ACE-FTS HNO_3 VMRs are 1.0–4.2 ppbv (typically 28%) larger than the SPIRALE VMRs. Larger differences are observed in the comparison with FIRS-2, varying from −3 ppbv at 16 and 28 km to +3 ppbv at 20 km. The mean relative differences oscillate between −55% and +50% and are typically 20%. All three airborne (SPIRALE, FIRS-2, and ASUR) measurements were performed in the Arctic winter during vortex conditions and show a minimum in HNO_3 at about 20 km, which results in a high bias for ACE-FTS of ∼2 ppbv which is not seen in the satellite comparisons. The SPIRALE and FIRS-2 data were affected by the presence of a PSC and may have seen local denitrification. However, the same degree of denitrification was not observed by ACE-FTS.

The last set of comparisons is with HNO_3 partial columns measured by the ground-based FTIRs. The mean relative differences are between −12.6% and +6.0%. The mean relative difference of all 122 FTIR coincidences is −1.3% with a standard deviation of ±25.9%, suggesting a slight negative bias in the ACE-FTS partial columns over the altitude regions being compared (∼15–30 km). No significant latitudinal bias could be detected.

Overall the quality of the ACE-FTS v2.2 HNO_3VMR profiles is good over the altitude range from 18 to 35 km. At lower altitudes, between 10 and 18 km, good agreement is seen between both MIPAS data products and ACE-FTS. As seen in Fig. 18, between 18 and 35 km, the mean absolute differences lie between −3.0 ppbv and +4.2 ppbv, with most values within ±1 ppbv. Mean relative differences are generally within ±20%, except for the aircraft and balloon high-latitude winter comparisons, which show values up to 45% smaller than ACE-FTS between 20 and 25 km. Based only on the MIPAS

and MLS comparisons, relative differences lie within ±10% between 10 and 36 km.

7.2 $ClONO_2$

ACE-FTS $ClONO_2$ profiles have been compared with the $ClONO_2$ measurements from the MIPAS satellite instrument (IMK-IAA data product) and from the FIRS-2 balloon flight. Partial column comparisons were performed with measurements by four ground-based FTIR instruments. Table 5 provides a summary of the profile comparisons. Good agreement between ACE-FTS and MIPAS IMK-IAA $ClONO_2$ is seen in the mean absolute differences, which are typically within ±0.01 ppbv and reach not more than −0.04 ppbv (±1%) for 16–27 km. ACE-FTS has a positive bias relative to CTM-corrected MIPAS IMK-IAA of about 0.09 ppbv (14%) between 27 and 34 km. We do not have an explanation for the large disagreement between the $ClONO_2$ profiles from ACE-FTS and the FIRS-2 balloon flight, which reaches −2.8 ppbv (−170%) at 24 km. These differences are under investigation.

The ground-based FTIR comparisons show varying degrees of agreement. Good agreement was found for the comparisons with the Jungfraujoch and Thule partial columns. The mean relative differences (given with standard error) are 4.7% ± 4.2% with standard deviation ±16.3% and −0.1% ± 8.7% with standard deviation ±28.9%, respectively. For the two Arctic stations, several coincident measurements in periods with high vortex variability (winter and spring) are included in the comparisons and hence may contribute to a larger scatter in the relative differences.

7.3 N_2O_5

ACE-FTS N_2O_5 profiles have been compared with the MIPAS IMK-IAA N_2O_5 data products and with the FIRS-2 balloon flight. Table 5 provides a summary of the profile comparisons. Between 16 and 27 km, ACE-FTS N_2O_5 VMRs differ by less than 0.04 ppbv from the CTM-corrected MIPAS IMK-IAA daytime measurements and by less than −0.09 ppbv from the CTM-corrected MIPAS IMK-IAA nighttime measurements. Rel-

ative differences show a low bias of typically −10% for the daytime comparisons and −27% for the nighttime comparisons. Above 27 km, the mean absolute differences increase and show a maximum low bias for ACE-FTS relative to MIPAS N_2O_5 of up to −0.25 ppbv (−44%) around 30 km. Because of the large uncertainties in the FIRS-2 N_2O_5 data, meaningful comparisons between ACE-FTS and FIRS-2 can only be obtained between 27 and 31 km. Over this region, ACE-FTS has a low bias of maximum −0.6 ppbv (∼51%).

To conclude, we have used all available data to assess the quality of three NO_y reservoirs measured by ACE-FTS. Only limited coincident measurements existed for $ClONO_2$ and N_2O_5, but a good set of statistical comparisons was obtained for HNO_3. If new correlative data become available in future, particularly for $ClONO_2$ and N_2O_5, further comparisons are recommended.

Acknowledgements. Funding for the ACE mission was provided primarily by the Canadian Space Agency (CSA) and the Natural Sciences and Engineering Research Council (NSERC) of Canada. This work was also supported by a grant from the CSA.

Odin is a Swedish-led satellite project funded jointly by the Swedish National Space Board (SNSB), the CSA, the Centre National d'Études Spatiales (CNES) in France and the National Technology Agency of Finland (Tekes).

Thanks to B. Bojkov of the Aura Validation Data Center (AVDC) and the Aura-MLS Data Distribution Team for access to the Aura-MLS dataset (see http://avdc.gsfc.nasa.gov). Work at the Jet Propulsion Laboratory, California Institute of Technology, is carried out under a contract with the National Aeronautics and Space Administration (NASA).

We acknowledge the European Space Agency (ESA) for providing the MIPAS level 1 and 2 datasets. We thank H. Fischer, U. Grabowski, S. Kellmann, M. Kiefer, A. Linden, M. Milz, T. Steck, G. P. Stiller, B. Funke, M. López–Puertas, and G. Mengistu-Tsidu from the MIPAS IMK-IAA team for their contributions and support.

The ASUR group would like to acknowledge help and support from H. Bremer, A. Kleinböhl and G. Naeveke.

The SPIRALE balloon measurements could only be performed thanks to the technical team (L. Pomathiod, B. Gaubicher, G. Jannet); the flight was funded by ESA and space French

agency CNES for the Envisat validation project; the CNES balloon launching team is greatly acknowledged for successful operations. A. Hauchecorne is acknowledged for making available the use of MIMOSA advection model and F. Coquelet for useful help in the PV calculations and ACE data formatting.

The FIRS-2 balloon measurements and data analysis was funded by the NASA Upper Atmosphere Program. The launch was supported both by the NASA Columbia Scientific Balloon Facility and the Swedish Space Corporation.

Eight of the ground-based FTIR stations operate within the framework of the Network for the Detection of Atmospheric Composition Change (NDACC, see http://www.ndacc.org). Poker Flat is a NDACC candidate and is currently under the process of becoming a complementary site. All stations are nationally funded and supported. The Belgian contributions to the present effort were supported by the ProDEx projects ACE, CINAMON and Envisat Database. The European ground-based FTIR stations have been supported partly by the EU project UFTIR (http://www.nilu.no/uftir). Thanks are extended to the "International Foundation High Altitude Research Stations Jungfraujoch and Gornergrat" (HFSJG, Bern, Switzerland) for hosting the Liège FTIR laboratory and for providing accommodation for the observers at the Jungfraujoch site. The support by the local IRF Kiruna staff is highly appreciated. The National Center for Atmospheric Research (NCAR) is supported by the National Science Foundation. The NCAR FTIR observation program at Thule, Greenland is supported under contract with NASA. The NIWA contribution to this study work was conducted within the FRST funded Drivers and Mitigation of Global Change programme (C01X0204). Support and logistics for measurements conducted at Arrival Heights was supplied by Antarctica New Zealand.

References

Abrams, M. C., Chang, A. Y., Gunson, M. R., Abbas, M. M., Goldman, A., Irion, F. W., Michelsen, H. A., Newchurch, M. J., Rinsland, C. P., Stiller, G. P., and Zander, R.: On the assessment and uncertainty of atmospheric trace gas burden measurements with high resolution infrared solar occultation spectra from space by the ATMOS experiment, Geophys. Res. Lett., 23, 2337–2340, doi:10.1029/96GL01794, 1996. 2434, 2436

Barret, B., Ricaud, P., Santee, M. L., Attié, J.-L., Urban, J., Flochmoën, E. L., Berthet, G., Murtagh, D., Eriksson, P., Jones, A., de La Noë, J., Dupuy, E., Froidevaux, L., Livesey, N. J.,

Waters, J. W., and Filipiak, M. J.: Intercomparisons of trace gas profiles from the Odin/SMR and Aura/MLS limb sounders, J. Geophys. Res., 111, D21302, doi:10.1029/2006JD007305, 2006. 2445

Bernath, P. F.: Atmospheric chemistry experiment (ACE): Analytical chemistry from orbit, Trends in Anal. Chem., 5, 647–654, 2006. 2437

Bernath, P. F., McElroy, C. T., Abrams, M. C., Boone, C. D., Butler, M., Camy-Peyret, C., Carleer, M., Clerbaux, C., Coheur, P. F., Colin, R., DeCola, P., Mazière, M. D., Drummond, J. R., Dufour, D., Evans, W. F. J., Fast, H., Fussen, D., Gilbert, K., Jennings, D. E., Llewellyn, E. J., Lowe, R. P., Mahieu, E., McConnel, J. C., McHugh, M., McLeod, S. D., Michaud, R., Midwinter, C., Nassar, R., Nichitu, F., Nowlan, C., Rinsland, C. P., Rochon, Y. J., Rowlands, N., Semeniuk, K., Simon, P., Skelton, R., Sloan, J. J., Soucy, M. A., Strong, K., Tremblay, P., Turnbull, D., Walker, K. A., Walkty, I., Wardle, D. A., Wehrle, V., Zander, R., and Zou, J.: Atmospheric Chemistry Experiment (ACE): Mission overview, Geophys. Res. Lett., 32, L15S01, doi:10.1029/2005GL022386, 2005. 2432, 2437

Bingham, G. E., Zhou, D. K., Bartschi, B. Y., Anderson, G. P., Smith, D. R., Chetwynd, J. H., and Nadile, R. M.: Cryogenic Infrared Radiance Instrumentation for Shuttle (CIRRIS 1A) Earth limb spectral measurements, calibration, and atmospheric O_3, HNO_3, CFC-12, and CFC-11 profile retrieval, J. Geophys. Res., 102, 3547–3558, 1997. 2434

Blumenstock, T., Kopp, G., Hase, F., Hochschild, G., Mikuteit, S., Raffalski, U., and Ruhnke, R.: Observation of unusual chlorine activation by ground-based infrared and microwave spectroscopy in the late Arctic winter 2000/01, Atmos. Chem. Phys., 6, 897–905, 2006, http://www.atmos-chem-phys.net/6/897/2006/. 2488

Boone, C. D., Nassar, R., Walker, K. A., Rochon, Y. J., McLeod, S. D., Rinsland, C. P., and Bernath, P. F.: Retrievals for the Atmospheric Chemistry Experiment Fourier-Transform Spectrometer, Appl. Optics, 44, 7218–7231, 2005. 2438

Brasseur, G. P. and Solomon, S.: Aeronomy of the Middle Atmosphere, Springer, Dordrecht, 3rd ed., XII, pp. 646, The Netherlands, 2005. 2432

Canty, T., Pickett, H. M., Salawitch, R. J., Jucks, K. W., Traub, W. A., and Waters, J. W.: Stratospheric and mesospheric HO_x: Results from Aura MLS and FIRS-2, Geophys. Res. Lett., 33, L12802, doi:10.1029/2006GL025964, 2006. 2458

Carli, B., Alpaslan, D., Carlotti, M., Castelli, E., Ceccherini, S., Dinelli, B. M., Dudhia, A., Flaud, J. M., Höpfner, M., Jay, V., Magnani, L., Oelhaf, H., Payne, V., Piccolo, C., Prosperi, M., Raspollini, P., Remedios, J., Ridolfi, M., and Spang, R.: First results of MIPAS/ENVISAT with

operational Level 2 code, Adv. Space Res., 33, 1012–1019, 2004. 2449
Dessler, A.: The Chemistry and Physics of Stratospheric Ozone, International Geophysics Series, Academic Press, Cornwall, IX, 214 pp., UK, 2000. 2433
Draxler, R. R. and Hess, G. D.: An Overview of the Hysplit_4 Modeling System for Trajectories, Dispersion, and Deposition, Aust. Met. Mag., 47, 295–308, 1998a. 2458
Draxler, R. R. and Hess, G. D.: Description of the Hysplit_4 modeling system, Tech. Rep. ERL ARL-224, NOAA, 1998b. 2458
Dunkerton, T. J. and Delisi, D. P.: Evolution of potential vorticity in the winter stratosphere of January–February 1979, J. Geophys. Res., 91, 1199–1208, 1986. 2459
Dupuy, E., Walker, K. A., Kar, J., Boone, C. D., McElroy, C. T., Bernath, P. F., Drummond, J. R., Skelton, R., McLeod, S. D., Hughes, R. C., Nowlan, C. R., Dufour, D. G., Zou, J., Nichitiu, F., Strong, K., Baron, P., Bevilacqua, R. M., Blumenstock, T., Bodeker, G. E., Borsdorff, T., Bourassa, A. E., Bovensmann, H., Boyd, I. S., Bracher, A., Brogniez, C., Burrows, J. P., Catoire, V., Ceccherini, S., Chabrillat, S., Christensen, T., Coffey, M. T., Cortesi, U., Davies, J., Clercq, C. D., Degenstein, D. A., Mazière, M. D., Demoulin, P., Dodion, J., Firanski, B., Fischer, H., Forbes, G., Froidevaux, L., Fussen, D., Gerard, P., Godin-Beekman, S., Goutail, F., Granville, J., Griffith, D., Haley, C. S., Hannigan, J. W., Höpfner, M., Jin, J. J., Jones, A., Jones, N. B., Jucks, K., Kagawa, A., Kasai, Y., Kerzenmacher, T. E., Kleinböhl, A., Klekociuk, A. R., Kramer, I., Küllmann, H., Kuttippurath, J., Kyrölä, E., Lambert, J. C., Livesey, N. J., Llewellyn, E. J., Lloyd, N. D., Mahieu, E., Manney, G. L., Marshall, B. T., McConnell, J. C., McCormick, M. P., McDermid, I. S., McHugh, M., McLinden, C. A., Mellqvist, J., Mizutani, K., Murayama, Y., Murtagh, D. P., Oelhaf, H., Parrish, A., Petelina, S. V., Piccolo, C., Pommereau, J. P., Randall, C. E., Robert, C., Roth, C., III, J. M. R., Schneider, M., Senten, C., Steck, T., Strandberg, A., Strawbridge, K. B., Sussmann, R., Swart, D. P. J., Tarasick, D. W., Taylor, J. R., Tétard, C., Thomason, L. W., Thompson, A. M., Tully, M. B., Urban, J., Vanhellemont, F., von Clarmann, T., von der Gathen, P., von Savigny, C., Waters, J. W., Witte, J. C., Wolff, M., and Zawodny, J. M.: Validation of ozone measurements from the Atmospheric Chemistry Experiment (ACE), Atmos. Chem. Phys. Discuss., accepted, 2007. 2442
Fischer, H., Birk, M., Blom, C., Carli, B., Carlotti, M., von Clarmann, T., Delbouille, L., Dudhia, A., Ehhalt, D., Endemann, M., Flaud, J. M., Gessner, R., Kleinert, A., Koopmann, R., Langen, J., López-Puertas, M., Mosner, P., Nett, H., Oelhaf, H., Perron, G., Remedios, J., Ridolfi, M., Stiller, G., and Zander, R.: MIPAS: an instrument for atmospheric and climate research, Atmos. Chem. Phys. Discuss., 7, 8795–8893, 2007,

http://www.atmos-chem-phys-discuss.net/7/8795/2007/. 2435, 2449
Froidevaux, L., Livesey, N. J., Read, W. G., Jiang, Y. B., Jimenez, C., Filipiak, M. J., Schwartz, M. J., Santee, M. L., Pumphrey, H. C., Jiang, J. H., Wu, D. L., Manney, G. L., Drouin, B. J., Waters, J. W., Fetzer, E. J., Bernath, P. F., Boone, C. D., Walker, K. A., Jucks, K. W., Toon, G. C., Margitan, J. J., Sen, B., Webster, C. R., Christensen, L. E., Elkins, J. W., Atlas, E., Lueb, R. A., and Hendershot, R.: Early validation analyses of atmospheric profiles from EOS MLS on the Aura Satellite, IEEE Trans. Geosci. Remote Sension, 44, 1106–1121, 2006. 2436
Gilbert, K. L., Turnbull, D. N., Walker, K. A., Boone, C. D., McLeod, S. D., Butler, M., Skelton, R., Bernath, P. F., Chateauneuf, F., and Soucy, M. A.: The onboard imagers for the Canadian ACE SCISAT-1 mission, J. Geophys. Res., 112, D12207, doi:10.1029/2006JD007714, 2007. 2437
Gille, J. C. and Russell, J. M.: The Limb Infrared Monitor of the Stratosphere: Experiment description, performance, and results, J. Geophys. Res., 89, 5125–5140, 1984. 2434
Gille, J. C., Bailey, P. L., Gandrud, B. W., Russell, J. M., Remsberg, E. E., Gordley, L. L., Evans, W. F. J., Fischer, H., Girard, A., and Harrison, J. E.: Accuracy and precision of the nitric acid concentrations determined by the Limb Infrared Monitor of the Stratosphere experiment on Nimbus 7, J. Geophys. Res., 89, 5179–5190, 1984. 2434
Gille, J. C., Barnett, J. J., Arter, P., Barker, M., Bernath, P. F., Boone, C. D., Cavanaugh, C., Chow, J., Coffey, M., Craft, J., Craig, C., Dials, M., Dean, V., Eden, T., Edwards, D. P., Francis, G., Halvorson, C., Harvey, L., Hepplewhite, C., Kinnison, D., Khosravi, R., Krinsky, C., Lambert, A., Lyjak, L., Lee, H., Loh, J., Mankin, W. G., McInnerney, J., Moorhous, J., Massie, S., Nardi, B., Packman, D., Randall, C. E., Reburn, J., Rudolf, W., Schwartz, M. J., Serafin, J., Stone, K., Torpy, B., Walker, K. A., Waterfall, A., Watkins, R., Whitney, J. G., Woodard, D., and Young, G.: The High Resolution Dynamics Limb Sounder (HIRDLS) Experiment Overview, Results and Temperature Validation, J. Geophys. Res., in review, 2007. 2435
Goldman, A., Paton-Walsh, C., Bell, W., Toon, G. C., Blavier, J. F., Sen, B., Coffey, M. T., Hannigan, J. W., and Mankin, W. G.: Network for the Detection of Stratospheric Change Fourier transform infrared intercomparison at Table Mountain Facility, J. Geophys. Res., 104, 30 481–30 504, 1999. 2488
Griffith, D. W. T., Jones, N. B., McNamara, B., Paton-Walsh, C., Bell, W., and Bernardo, C.: Intercomparison of ground-based solar FTIR measurements of atmospheric gases at Lauder, New Zealand, J. Atmos. Oceanic Technol., 20, 1138–1153, 2003. 2488

Gunson, M. R., Abbas, M. M., Abrams, M. C., Allen, M., Brown, L. R., Brown, T. L., Chang, A. Y., Goldman, A., Irion, F. W., Lowes, L. L., Mahieu, E., Manney, G. L., Michelsen, H. A., Newchurch, M. J., Rinsland, C. P., Salawitch, R. J., Stiller, G. P., Toon, G. C., Yung, Y. L., and Zander, R.: The Atmospheric Trace Molecule Spectroscopy (ATMOS) experiment: Deployment on the ATLAS Space Shuttle missions, Geophys. Res. Lett., 23, 2333–2336, 1996. 2434, 2436

Hase, F.: Inversion von Spurengasprofilen aus hochaufgelösten bodengebundenen FTIR-Messungen in Absorption – Retrieval of trace gas profiles from high resolution, ground based FTIR-measurements in absorption, 6512, FZKA Wissenschaftliche Berichte – Scientific Reports, Forschungszentrum Karlsruhe, 2000. 2461

Hase, F., Hannigan, J. W., Coffey, M. T., Goldman, A., Höpfner, M., Jones, N. B., Rinsland, C. P., and Wood, S. W.: Intercomparison of retrieval codes used for the analysis of high-resolution, ground-based FTIR measurements, J. Quant. Spectrosc. Radiat. Transfer, 87, 25–52, doi:10.1016/j.jqsrt.2003.12.008, 2004. 2461

Hauchecorne, A., Godin, S., Marchand, M., Heese, B., and Souprayen, C.: Quantification of the transport of chemical constituents from the polar vortex to midlatitudes in the lower stratospher using the high-resolution advection model MIMOSA and effective diffusivity, J. Geophys. Res., 107, 8289, doi:10.1029/2001JD000491, 2002. 2457

Hofmann, D. J. and Solomon, S.: Ozone destruction through heterogeneous chemistry following the eruption of El Chichón, J. Geophys. Res., 94, 5029–5041, 1989. 2434

Höpfner, M., von Clarmann, T., Fischer, H., Funke, B., Glatthor, N., Grabowski, U., Kellmann, S., Kiefer, M., Linden, A., Milz, M., Steck, T., Stiller, G. P., Bernath, P. F., Blom, C. E., Blumenstock, T., Boone, C., Chance, K., Coffey, M. T., Friedl-Vallon, F., Griffith, D., Hannigan, J. W., Hase, F., Jones, N., Jucks, K. W., Keim, C., Kleinert, A., Kouker, W., Liu, G. Y., Mahieu, E., Mellqvist, J., Mikuteit, S., Notholt, J., Oelhaf, H., Piesch, C., Reddmann, T., Ruhnke, R., Schneider, M., Strandberg, A., Toon, G., Walker, K. A., Warneke, T., Wetzel, G., Wood, S., and Zander, R.: Validation of MIPAS $ClONO_2$ measurements, Atmos. Chem. Phys., 7, 281, 2007. 2435, 2436, 2451, 2452, 2465

Irie, H., Kondo, Y., Koike, M., Danilin, M. Y., Camy-Peyret, C., Payan, S., Pommereau, J. P., Goutail, F., Oelhaf, H., Wetzel, G., Toon, G. C., Sen, B., Bevilacqua, R. M., III, J. M. R., Renard, J. B., Kanzawa, H., Nakajima, H., Yokota, T., Sugita, T., and Sasano, Y.: Validation of NO_2 and HNO_3 measurements from the Improved Limb Atmospheric Spectrometer (ILAS) with the version 5.20 retrieval algorithm, J. Geophys. Res., 107, 8206, doi:

10.1029/2001JD001304, 2002. 2435
Irie, H., Sugita, T., Nakajima, H., Yokota, T., Oelhaf, H., Wetzel, G., Toon, G. C., Sen, B., Santee, M. L., Terao, Y., Saitoh, N., Ejiri, M. K., Tanaka, T., Kondo, Y., Kanzawa, H., Kobayashi, H., and Sasano, Y.: Validation of stratospheric nitric acid profiles observed by Improved Limb Atmospheric Spectrometer (ILAS)-II, J. Geophys. Res., 111, D11S03, doi:10.1029/2005JD006115, 2006. 2435
Irion, F. W., Gunson, M. R., Toon, G. C., Chang, A. Y., Eldering, A., Mahieu, E., Manney, G. L., Michelsen, H. A., Moyer, E. J., Newchurch, M. J., Osterman, G. B., Rinsland, C. P., Salawitch, R. J., Sen, B., Yung, Y. L., and Zander, R.: Atmospheric Trace Molecule Spectroscopy (ATMOS) Experiment Version 3 data retrievals, Appl. Optics, 41, 6968–6979, 2002. 2434
Johnson, D. G., Jucks, K. W., Traub, W. A., and Chance, K. V.: Smithsonian stratospheric far-infrared spectrometer and data reduction system, J. Geophys. Res., 100, 3091–3106, doi:10.1029/94JD02685, 1995. 2458, 2459
Jucks, K. W., Johnson, D. G., Chance, K. V., Traub, W. A., Margitan, J. M., Stachnik, R., Sasano, Y., Yokota, T., Kanzawa, H., Shibasaki, K., Suzuki, M., and Ogawa, T.: Validation of ILAS v5.2 data with FIRS-2 balloon observations, J. Geophys. Res., 107, 8207, doi:10.1029/2001JD000578, 2002. 2458, 2459
Kasai, Y. J., Kagawa, A., Jones, N., Fujiwara, A., Seki, K., Murayama, Y., and Murcray, F.: Seasonal variations of CO and HCN in the troposphere measured by solar absorption spectroscopy over Poker Flat, Alaska, Geophys. Res. Lett., 32, L19812, doi:10.1029/2005GL022826, 2005. 2488
Kerzenmacher, T., Wolff, M. A., Strong, K., Dupuy, E., Walker, K. A., Amekudzi, L. K., Batchelor, R. L., Bernath, P. F., Berthet, G., Blumenstock, T., Boone, C. D., Bramstedt, K., Brogniez, C., Brohede, S., Burrows, J. P., Catoire, V., Dodion, J., Drummond, J. R., Dufour, D. G., Funke, B., Fussen, D., Goutail, F., Griffith, D. W. T., Haley, C. S., Hendrick, F., Höpfner, M., Huret, N., Jones, N. B., Kar, J., Kramer, I., Llewellyn, E. J., López-Puertas, M., Manney, G. L., McElroy, C. T., McLinden, C. A., Melo, S., Mikuteit, S., Murtagh, D. P., Nichitiu, F., Notholt, J., Nowlan, C. R., Piccolo, C., Pommereau, J. P., Randall, C. E., Richter, A., Schneider, M., Schrems, O., Silicani, M., Stiller, G. P., Taylor, J. R., Tétard, C., Toohey, M., Vanhellemont, F., Warneke, T., Zawodny, J. M., and Zou, J.: Validation of NO_2 and NO from the Atmospheric Chemistry Experiment (ACE), Atmos. Chem. Phys. Discuss., accepted, 2007. 2432
King, P., McKinnon, I. R., Mathieson, J. G., and Wilson, I. R.: Upper limit to stratospheric N_2O_5 abundance, J. Atmos. Sci., 33, 1657–1659, 1976. 2436

Kinnison, D. E., Gille, J., Barnett, J., Randall, C., Harvey, L., Lambert, A., Khosravi, R., Alexander, M. J., Bernath, P. F., Boone, C. D., Cavanaugh, C., Coffey, M., Craig, C., Dean, V. C., Eden, T., Ellis, D., Fahey, D. W., Francis, G., Halvorson, C., Hannigan, J., Hartsough, C., Hepplewhite, C., Krinsky, C., Lee, H., Mankin, B., Marcy, T. P., Massie, S., Nardi, B., Packman, D., Popp, P. J., Santee, M. L., and Walker, K. A.: Global Observations of HNO_3 from the High Resolution Dynamics Limb Sounder (HIRDLS) - First results, J. Geophys. Res., in review, 2007. 2435, 2436

Kleinböhl, A., Bremer, H., von König, M., Küllmann, H., Künzi, K., Goede, A. P. H., v. Browell, E., Grant, W. B., Toon, G. C., Blumenstock, T., Galle, B., Sinnhuber, B. M., and Davies, S.: Vortexwide denitrification of the Arctic polar stratosphere in winter 1999/2000 determined by remote observations, J. Geophys. Res., 108, doi:10.1029/2001JD001042, 2003. 2455

Kleinböhl, A., Bremer, H., Küllmann, H., Kuttippurath, J., Browell, E. V., Canty, T., Salawitch, R. J., Toon, G. C., and Notholt, J.: Denitrification in the Arctic mid-winter 2004/2005 observed by airborne submillimeter radiometry, Geophys. Res. Lett., 32, doi:10.1029/2005/Gl023408, 2005. 2455

Koike, M., Kondo, Y., Irie, H., Murcray, F. J., Williams, J., Fogal, P., Blatherwick, R., Camy-Peyret, C., Payan, S., Oelhaf, H., Wetzel, G., Traub, W., Johnson, D., Jucks, K., Toon, G. C., Sen, B., Blavier, J. F., Schlager, H., Ziereis, H., Toryama, N., Danilin, M. Y., Rodriguez, J. M., Kanzawa, H., and Sasano, Y.: A comparison of Arctic HNO_3 profiles measured by the Improved Limb Atmospheric Spectrometer and balloon-borne sensors., J. Geophys. Res., 105, 6761–6771, 2000. 2435

Kouker, W., Langbein, I., Reddmann, T., and Ruhnke, R.: The Karlsruhe simulation model of the middle atmosphere (KASIMA), version 2, 6278, FZKA Wissenschaftliche Berichte – Scientific Reports, Forschungszentrum Karlsruhe, 1999. 2451, 2454

Kumer, J. B., Mergenthaler, J. L., Roche, A. E., Nightingale, R. W., Ely, G. A., Uplinger, W. G., Gille, J. C., Massie, S. T., Bailey, P. L., Gunson, M. R., Abrams, M. C., Toon, G. C., Sen, B., Blavier, J., Stachnik, R. A., Webster, C. R., May, R. D., Murcray, D. G., Murcray, F. J., Goldman, A., Traub, W. A., Jucks, K. W., and Johnson, D. G.: Comparison of correlative data with HNO_3 version 7 from the CLAES instrument deployed on the NASA Upper Atmosphere Research Satellite, J. Geophys. Res., 101, 9621–9656, doi:10.1029/95JD03759, 1996a. 2434

Kumer, J. B., Mergenthaler, J. L., Roche, A. E., Nightingale, R. W., Zele, F., Gille, J. C., Massie, S. T., Bailey, P. L., Connell, P. S., Gunson, M. R., Abrams, M. C., Toon, G. C., Sen, B.,

Blavier, J., Smith, S. E., and Taylor, F. W.: Comparison of CLAES preliminary N_2O_5 data with correlative data and a model, J. Geophys. Res., 101, 9657–9677, 1996b. 2436

Kumer, J. B., Kawa, S. R., Roche, A. E., Mergenthaler, J. L., Smith, S. E., Taylor, F. W., Connell, P. S., and Douglass, A. R.: UARS first global N_2O_5 data sets: Application to a stratospheric warming event in January 1992, J. Geophys. Res., 102, 3575–3582, 1997. 2436

Livesey, N. J., Snyder, W. V., Read, W. G., and Wagner, P. A.: Retrieval algorithms for the EOS Microwave limb sounder (MLS), IEEE Trans. Geosci. Remote Sens., 44, 1144–1155, doi:10.1109/TGRS.2006.872327, 2006. 2447

Livesey, N. J., Read, W. G., Lambert, A., Cofield, R. E., Cuddy, D. T., Froidevaux, L., Fuller, R. A., Jarnot, R. F., Jiang, J. H., Jiang, Y. B., Knosp, B. W., Kovalenko, L. J., Pickett, H. M., Pumphrey, H. C., Santee, M. L., Schwartz, M. J., Stek, P. C., Wagner, P. A., Waters, J. W., and Wu, D. L.: Earth Observing System (EOS)– Aura Microwave Limb Sounder (MLS), Version 2.2 Level 2 data quality and description document, Tech. Rep. JPL D-33509, Jet Propulsion Laboratory, California Institute of Technology, 2007. 2447

Mahieu, E., Zander, R., Delbouille, L., Demoulin, P., Roland, G., C., and Servais: Observed trends in total vertical column abundances of atmospheric gases from IR solar spectra recorded at the Jungfraujoch, J. Atmos. Chem., 28, 227–243, 1997. 2488

Mahieu, E., Zander, R., Duchatelet, P., Hannigan, J. W., Coffey, M. T., Mikuteit, S., Hase, F., Blumenstock, T., Wiacek, A., Strong, K., Taylor, J. R., Mittermeier, R. L., Fast, H., Boone, C. D., McLeod, S. D., Walker, K. A., Bernath, P. F., and Rinsland, C. P.: Comparisons between ACE-FTS and ground-based measurements of stratospheric HCL and $ClONO_2$ loadings at northern latitudes, Geophys. Res. Lett., 32, L15S08, doi:10.1029/2005GL022396, 2005. 2436

Manney, G. L., Zurek, R. W., O'Neill, A., and Swinbank, R.: On the motion of air through the stratospheric polar vortex, J. Atmos. Sci., 51, 2973–2994, 1994. 2459

McElroy, C. T., Nowlan, C. R., Drummond, J. R., Bernath, P. F., Barton, D. V., Dufour, D. G., Midwinter, C., Hall, R. B., Ogyu, A., Ullberg, A., Wardle, D. I., Kar, J., Zou, J., Nichitiu, F., Boone, C. D., Walker, K. A., and Rowlands, N.: The ACE-MAESTRO instrument on SCISAT: Description, performance, and preliminary results, Appl. Optics, 46, 4341–4356, 2007. 2432, 2437

McLinden, C. A., Olsen, S. C., Hannegan, B., Wild, O., Prather, M. J., and Sundet, J.: Stratospheric ozone in 3-D models: A simple chemistry and the cross-tropopause flux, J. Geophys. Res., 105, 14 653–14 665, 2000. 2457

Mengistu Tsidu, G., von Clarmann, T., Stiller, G. P., Höpfner, M., Fischer, H., Glatthor, N., Grabowski, U., Kellmann, S., Kiefer, M., Linden, A., Milz, M., Steck, T., Wang, D. Y., and Funke, B.: Stratospheric N_2O_5 in the austral spring 2002 as retrieved from limb emission spectra recorded by the Michelson Interferometer for Passive Atmospheric Sounding (MIPAS), J. Geophys. Res., 109, D11301, doi:10.1029/2004JD004856, 2004. 2436, 2453

Mengistu Tsidu, G., Stiller, G. P., von Clarmann, T., Funke, B., Höpfner, M., Fischer, H., Glatthor, N., Grabowski, U., Kellmann, S., Kiefer, M., Linden, A., López-Puertas, M., Milz, M., Steck, T., and Wang, D. Y.: NOy from Michelson Interferometer for Passive Atmospheric Sounding on Environmental Satellite during the Southern Hemisphere polar vortex split in September/October 2002., J. Geophys. Res., 110, D18301, doi:10.1029/2004JD005322, 2005. 2435

Mergenthaler, J. L., Kumer, J. B., Roche, A. E., Nightingale, R. W., Potter, J. F., Gille, J. C., Massie, S. T., Bailey, P. L., Edwards, D., Connell, P. S., Kinnison, D. E., Gunson, M. R., Abrams, M. C., Toon, G. C., Sen, B., Blavier, J. F., Murcray, D. G., Murcray, F. J., and Goldman, A.: Validation of CLAES $ClONO_2$ measurements, J. Geophys. Res., 101, 9603–9620, 1996. 2435

Moreau, G., Robert, C., Catoire, V., Chartier, M., Camy-Peyret, C., Huret, N., Pirre, M., Pomathiod, L., and Chalumeau, G.: SPIRALE: a multispecies in situ balloon-borne instruments with six tunable diode laser spectrometers, Appl. Optics, 44, 5972–5989, 2005. 2456

Murcray, D. G., Kyle, T. G., Murcray, F. H., and Williams, W. J.: Nitric acid and nitric oxide in the lower stratosphere, Nature, 218, 78–79, 1968. 2434

Murcray, D. G., Goldman, A., Murcray, F. H., Murcray, F. J., and Williams, W. J.: Stratospheric distribution of $ClONO_2$, Geophys. Res. Lett., 6, 857–859, 1979. 2435

Murtagh, D., Frisk, U., Merino, F., Ridal, M., Jonsson, A., Stegman, J., Witt, G., Eriksson, P., Jiménez, C., Mégie, G., de la Nöe, J., Ricaud, P., Baron, P., Pardo, J. R., Hauchcorne, A., Llewellyn, E. J., Degenstein, D. A., Gattinger, R. L., Lloyd, N. D., Evans, W. F. J., McDade, I. C., Haley, C. S., Sioris, C., von Savigny, C., Solheim, B. H., McConnell, J. C., Strong, K., Richardson, E. H., Leppelmeier, G. W., Kyrölä, E., Auvinen, H., and Oikarinen, L.: An overview of the Odin atmospheric mission, Can. J. Phys., 80, 309–319, 2002. 2435, 2445

Nakajima, H., Suzuki, M., Matsuzaki, A., Ishigaki, T., Waragai, K., Mogi, Y., Kimura, N., Araki, N., Yokota, T., Kanzawa, H., Sugita, T., and Sasano, Y.: Characteristics and performance of the Improved Limb Atmospheric Spectrometer (ILAS) in orbit, J. Geophys. Res., 107, 8213, doi:10.1029/2001JD001439, 2002. 2435, 2458

Nakajima, H., Sugita, T., Irie, H., Saitoh, N., Kanzawa, H., Oelhaf, H., Wetzel, G., Toon, G. C.,

Sen, B., Blavier, J. F., Traub, W. A., Jucks, K., Johnson, D. G., Yokota, T., Yokota, T., and Sasano, Y.: Measurements of $ClONO_2$ by the Improved Limb Atmospheric Spectrometer (ILAS) in high-latitude stratosphere: New products using version 6.1 data processing algorithm, J. Geophys. Res., 111, D11S09, doi:10.1029/2005JD006441, 2006. 2435

Nash, E. R., Newman, P. A., Rosenfield, J. E., and Schoeberl, M. R.: An objective determination of the polar vortex using Ertel's potential vorticity, J. Geophys. Res., 101, 9471–9478, 1996. 2456

Offermann, D., Grossmann, K. U., Barthol, P., Knieling, P., Riese, M., and Trant, R.: Cryogenic Infrared Spectrometers and Telescopes for the Atmosphere (CRISTA) experiment and middle atmosphere variability, J. Geophys. Res., 104, 16, 3251, 1999. 2434, 2435

Oshchepkov, S., Sasano, Y., Yokota, T., Nakajima, H., Uemura, N., Saitoh, N., Sugita, T., and Matsuda, H.: ILAS data processing for stratospheric gas and aerosol retrievals with aerosol physical modeling: Methodology and validation of gas retrievals, J. Geophys. Res., 111, D02307, doi:10.1029/2005JD006543, 2006. 2436

Paton-Walsh, C., Jones, N. B., Wilson, S. R., Haverd, V., Meier, A., Griffith, D. W. T., and Rinsland, C. P.: Measurements of trace gas emissions from Australian forest fires and correlations with coincident measurements of aerosol optical depth, J. Geophys. Res., 110, D24305, doi:24310.21029/22005JD006202, 2005. 2488

Pougatchev, N. S. and Rinsland, C. P.: Spectroscopic study of the seasonal variation of carbon monoxide vertical distribution above Kitt Peak, J. Geophys. Res., 100, 1409–1416, 1995. 2461

Pougatchev, N. S., Connor, B. J., and Rinsland, P. C.: Infrared measurements of the ozone vertical distribution above Kitt Peak, J. Geophys. Res., 100, 16 689–16 698, 1995. 2461

Raspollini, P., Belotti, C., Burgess, A., Carli, B., Carlotti, M., Ceccherini, S., Dinelli, B. M., Dudhia, A., Flaud, J. M., Funke, B., Höpfner, M., López-Puertas, M., Payne, V., Piccolo, C., Remedios, J., Ridolfi, M., and Spang, R.: MIPAS level 2 operational analysis, Atmos. Chem. Phys., 6, 5605–5630, 2006, http://www.atmos-chem-phys.net/6/5605/2006/. 2449

Reisinger, A. R., Jones, N. B., Matthews, W. A., and Rinsland, C. P.: Southern hemisphere midlatitude ground-based measurements of $ClONO_2$, J. Geophys. Res., 100, 23 183–23 194, doi:10.1029/95JD02529, 1995. 2464

Ridolfi, M., Carli, B., Carlotti, M., von Clarmann, T., Dinelli, B., Dudhia, A., Flaud, J. M., Höpfner, M., Morris, P. E., Raspollini, P., Stiller, G., and Wells, R. J.: Optimized forward and retrieval

scheme for MIPAS near-real-time data processing, Appl. Optics, 39, 1323–1340, 2000. 2449
Riese, M., Preusse, P., Spang, R., Ern, M., Jarisch, M., Grossmann, K. U., and Offermann, D.: Measurements of trace gases by the Cryogenic Infrared Spectrometers and Telescopes for the Atmosphere (CRISTA) experiment, Adv. Space Res., 19, 563–566, 1997. 2436
Riese, M., Spang, R., Preusse, P., Ern, M., Jarisch, M., Offermann, D., and Grossmann, K. U.: Cryogenic Infrared Spectrometers and Telescopes for the Atmosphere (CRISTA) data processing and atmospheric temperature and trace gas retrieval, J. Geophys. Res., 104, 16 349–16 368, 1999. 2434, 2435, 2436
Rinsland, C. P., Goldman, A., Murcray, D. G., Murcray, F. J., and Devi, V. M.: Tentative identification of the 780 cm^{-1} ν_4 band Q branch of chlorine nitrate in high-resolution solar absorption spectra of the stratosphere, J. Geophys. Res., 90, 7931–7943, 1985. 2435
Rinsland, C. P., Zander, R., and Demoulin, P.: Ground-based infrared measurements of HNO_3 total column abundances: long-term trend and variability, J. Geophys. Res., 96, 9379–9389, 1991. 2434
Rinsland, C. P., Gunson, M. R., Abrams, M. C., Zander, R., Mahieu, E., Goldman, A., Ko, M. K. W., Rodriguez, J. M., and Sze, N. D.: Profiles of stratospheric chlorine nitrate ($ClONO_2$) from atmospheric trace molecule spectroscopy/ATLAS 1 infrared solar occultation spectra, J. Geophys. Res., 99, 18 895–18 900, 1994. 2435
Rinsland, C. P., Gunson, M. R., Salawitch, R. J., Michelsen, H. A., Zander, R., Newchurch, M. J., Abbas, M. M., Abrams, M. C., Manney, G. L., Chang, A. Y., Irion, F. W., Goldman, A., and Mahieu, E.: ATMOS/ATLAS-3 measurements of stratospheric chlorine and reactive nitrogen partitioning inside and outside the November 1994 Antarctic vortex, Geophys. Res. Lett., 23, 2365–2368, 1996. 2435
Rinsland, C. P., Jones, N. B., Connor, B. J., Logan, J. A., Pougatchev, N. S., Goldman, A., Murcray, F. J., Stephen, T. M., Pine, A. S., Zander, R., Mahieu, E., P., and Demoulin: Northern and Southern Hemisphere ground-based infrared spectroscopic measurements of tropospheric carbon monoxide and ethane, J. Geophys. Res., 103, 28 197–28 217, 1998. 2461
Roche, A., Kumer, J., Mergenthaler, J., Ely, G., Uplinger, W., Potter, J., James, T., and Sterritt, L.: The Cryogenic Limb Array Etalon Spectrometer (CLAES) on UARS: Experiment description and performance, J. Geophys. Res., 98, 10 763–10 775, 1993. 2434
Roche, A. E., Kumer, J. B., Mergenthaler, J. L., Nightingale, R. W., Uplinger, W. G., Ely, G. A., and Potter, J. F.: Observations of lower-stratospheric $ClONO_2$, HNO_3, and aerosol by the UARS CLAES experiment between January 1992 and April 1993, J. Atmos. Sci., 51, 2877–

2902, 1994. 2434
Rodgers, C. D.: Inverse Methods for Atmospheric Sounding, Theory and Praxis, vol. 2 of Series on Atmospheric, Oceanic and Planetary Physics, World Scientific, 2000. 2455, 2462
Rodgers, C. D. and Connor, B. J.: Intercomparison of remote sounding instruments, J. Geophys. Res., 108, 4116, doi:10.1029/2002JD002299, 2003. 2442, 2462
Roscoe, H. K.: Review and revision of measurements of stratospheric N_2O_5, J. Geophys. Res., 96, 10 879–10 884, doi:10.1029/90JD02388, 1991. 2436
Rothman, L. S., Jacquemart, D., Barbe, A., Benner, D. C., Birk, M., Brown, L. R., Carleer, M. R., Chackerian, C., Chance, C., Coudert, L. H., Dana, V., Devi, V. M., Flaud, J. M., Gamache, R. R., Goldman, A., Hartmann, J. M., Jucks, K. W., Maki, A. G., Mandin, J. Y., Massie, S. T., Orphal, J., Perrin, A., Rinsland, C. P., Smith, M. A. H., Tennyson, J., Tolchenov, R. N., Toth, R. A., Auwera, J. V., Varanasi, P., and Wagner, G.: The HITRAN 2004 molecular spectroscopic database, J. Quant. Spectrosc. Radiat. Transfer, 96, 139–204, doi:10.1016/j.jqsrt.2004.10.008, 2005. 2438, 2453, 2456, 2463, 2464
Schneider, M., Blumenstock, T., Chipperfield, M., Hase, F., Kouker, W., Reddmann, T., Ruhnke, R., Cuevas, E., and Fischer, H.: Subtropical trace gas profiles determined by ground-based FTIR spectroscopy at Izaña (28° N, 16° W): Five year record, error analysis, and comparison with 3D-CTMs, Atmos. Chem. Phys., 5, 153–167, 2005, http://www.atmos-chem-phys.net/5/153/2005/. 2488
Salawitch, R. J., Wofsy, S. C., Wennberg, P. O., Cohen, R. C., Anderson, J. G., Fahey, D. W., Gao, R. S., Keim, E. R., Woodbridge, E. L., Stimpfle, R. M., Koplow, J. P., Kohn, D. W., Webster, C. R., May, R. D., Pfister, L., Gottlieb, E. W., Michelsen, H. A., Yue, G. K., Prather, M. J., Wilson, J. C., Brock, C. A., Jonsson, H. H., Dye, J. E., Baumgardner, D., Proffitt, M. H., Loewenstein, M., Podolske, J. R., Elkins, J. W., Dutton, G. S., Hintsa, E. J., Dessler, A. E., Weinstock, E. M., Kelly, K. K., Boering, K. A., Daube, B. C., Chan, K. R., and Bowen, S. W.: The diurnal variation of hydrogen, nitrogen, and chlorine radicals: Implications for the heterogeneous production of HNO_3, Geophys. Res. Lett., 21, 2551–2554, 1994. 2433
Santee, M. L., Manney, G. L., Froidevaux, L., Read, W. G., and Water, J. W.: Six years of UARS Microwave Limb Sounder HNO_3 observations: Seasonal, interhemispheric, and interannual variations in the lower stratosphere, J. Geophys. Res., 104, 8225–8246, 1999. 2434
Santee, M. L., Manney, G. L., Livesey, N. J., and Read, W. G.: Three-dimensional structure and evolution of stratospheric HNO_3 based on UARS Microwave Limb Sounder measurements, J. Geophys. Res., 109, doi:101029/2004JD004578, 2004. 2434, 2448

Santee, M. L., Lambert, A., Read, W. G., Livesey, N. J., Cofield, R. E., Cuddy, D. T., Daffer, W. H., Drouin, B. J., Froidevaux, L., Fuller, R. A., Jarnot, R. F., Knosp, B. W., Manney, G. L., Perun, V. S., Snyder, W. V., Stek, P. C., Thurstans, R. P., Wagner, P. A., Waters, J. W., Muscari, G., de Zafra, R. L., Dibb, J. E., Fahey, D. W., Popp, P. J., Marcy, T. P., Jucks, K. W., Toon, G. C., Stachnik, R. A., Bernath, P. F., Boone, C. D., Walker, K. A., Urban, J., and Murtagh, D.: Validation of the Aura Microwave Limb Sounder HNO_3 Measurements, J. Geophys. Res., in press, doi:10.1029/2007JD008721, 2007. 2435, 2436, 2446, 2447, 2448, 2467

Senten, C., Mazière, M. D., Dils, B., Hermans, C., Kruglanski, M., Neefs, E., Scolas, F., Vandaele, A. C., Vanhaelewyn, G., Vigouroux, C., Carleer, M., Coheur, P. F., Fally, S., Barret, B., Baray, J. L., Delmas, R., Leveau, J., Metzger, J. M., Mahieu, E., Boone, C., Walker, K. A., Bernath, P. F., and Strong, K.: New ground-based FTIR measurements at Ile de La Réunion: Observations, error analysis, and comparisons with independent data, Atmos. Chem. Phys., submitted, 2007. 2488

Smith, S. E., Dudhia, A., Morris, P. E., Remedios, J. J., Rodgers, C. D., Taylor, F. W., Kerridge, B. J., Chipperfield, M. P., Kumer, J. B., Roche, A. E., and Gunson, M. R.: Dinitrogen pentoxide measurements from the Improved Stratospheric And Mesospheric Sounder: Validation of preliminary results, J. Geophys. Res., 101, 9897–9906, doi:10.1029/95JD02465, 1996. 2436

Solomon, S.: Stratospheric Ozone Depletion: A review of concepts and history, Rev. Geophys., 37, 275–316, 1999. 2432

Solomon, S., Portmann, R. W., Garcia, R. R., Thomason, L. W., Poole, L. R., and McCormick, M. P.: The role of aerosol variations in anthropogenic ozone depletion at northern midlatitudes, J. Geophys. Res., 101, 6713–6727, 1996. 2433

Stiller, G. P., Tsidu, G. M., von Clarmann, T., Glatthor, N., Höpfner, M., Kellmann, S., Linden, A., Ruhnke, R., and Fischer, H.: An enhanced HNO_3 second maximum in the Antarctic mid-winter upper stratosphere 2003, J. Geophys. Res., 110, D20303, doi:10.1029/2005JD006011, 2005. 2435

Strong, K., Wolff, M. A., Kerzenmacher, T. E., Walker, K. A., Bernath, P. F., Blumenstock., T., Boone, C., Catoire, V., Coffey, M., Mazière, M. D., Demoulin, P., Duchatelet, P., Dupuy, E., Hannigan, J., Höpfner, M., Glatthor, N., Griffith, D. W. T., Jin, J. J., Jones, N., Jucks, K., Kuttippurath, J., Lambert, A., Mahieu, E., McConnell, J. C., Mellqvist, J., Mikuteit, S., Murtagh, D. P., Notholt, J., Piccolo, C., Robert, C., Schneider, M., Schrems, O., Semeniuk, K., Senten, C., Stiller, G. P., Strandberg, A., Taylor, J. R., Tétard, C., Toohey, M., Urban,

J., Warneke, T., and Wood, S.: Validation of ACE-FTS N_2O Measurements, Atmos. Chem. Phys. Discuss., accepted, 2007. 2432

Taylor, F. W., Rodgers, C. D., Whitney, J. G., Werrett, S. T., Barnett, J., Peskett, G. D., Venters, P., Ballard, J., Palmer, C. W. P., Knight, R. J., Morris, P., Nightingale, T., and Dudhia, A.: Remote sensing of atmospheric structure and composition by pressure modulator radiometry from space: The ISAMS experiment on UARS, J. Geophys. Res., 98, 10 799–10 814, 1993. 2434, 2436

Taylor, F. W., Ballard, J., Dudhia, A., Goss-Custard, M., Kerridge, B., Lambert, A., López-Valverde, M., Rodgers, C., and Remedios, J.: Stratospheric and mesospheric observations with ISAMS, Adv. Space Res., 14, 41–52, 1994. 2434

Taylor, F. W., Rodgers, C., Remedios, J., Grainger, R., Lambert, A., López-Valverde, M., Goss-Custard, M., and Reburn, J.: Global atmospheric chemistry from satellites: Results from UARS/ISAMS, Faraday Discuss., 100, 353–369, 1995. 2434

Toohey, M. and Strong, K.: Estimating biases and error variances through the comparison of coincident satellite measurements, J. Geophys. Res., 112, D13306, doi:10.1029/2006JD008192, 2007. 2436

Toohey, M., Quine, B. M., Strong, K., Bernath, P. F., Boone, C. D., Jonsson, A. I., McElroy, C. T., Walker, K. A., and Wunch, D.: Balloon-borne radiometer measurement of Northern Hemisphere mid-latitude stratospheric HNO_3 profiles spanning 12 years, Atmos. Chem. Phys. Discuss., 7, 11 561–11 586, 2007. 2436

Toon, O. B., Hamill, P., Turco, R. P., and Pinto, J.: Condensation of HNO_3 and HCl in the winter polar stratosphere, Geophys. Res. Lett., 13, 1284–1287, 1986. 2434

Urban, J., Lautié, N., Flochmoën, E. L., Jiménez, C., Eriksson, P., Dupuy, E., Amaroui, L. E., Ekström, M., Frisk, U., Murtagh, D. P., de La Noë, J., Olberg, M., and Ricaud, P.: Odin/SMR Limb Observations of Stratospheric Trace Gases: Level 2 Processing of ClO, N_2O, O_3, and HNO_3, J. Geophys. Res., 110, D14307, doi:10.1029/2004JD005741, 2005. 2435, 2445

Urban, J., Murtagh, D. P., Lautié, N., Barret, B., Dupuy, E., de Noë, L., Eriksson, P., Frisk, U., Jones, A., E., F. L., Olberg, M., Piccolo, C., Ricaud, P., and Rösevall, J.: Odin/SMR Limb Observations of Trace Gases in the Polar Lower Stratosphere during 2004-2005, in: Proc. ESA First Atmospheric Science Conference, edited by Lacoste, H., ESA-SP-628, European Space Agency, 2006. 2445

Urban, J., Pommier, M., Murtagh, D. P., Eriksson, P., and Ricaud, P.: Odin/SMR Limb Observations of Nitric Acid in the Stratosphere, in: Proc. ESA Envisat Symposium, edited by Lacoste,

H. and Ouwehand, L., ESA-SP-636, European Space Agency, 2007. 2445
Vigouroux, C., Mazière, M. D., Errera, Q., Chabrillat, S., Mahieu, E., Duchatelet, P., Wood, S., Smale, D., Mikuteit, S., Blumenstock, T., Hase, F., and Jones, N.: Comparisons between ground-based FTIR and MIPAS N_2O and HNO_3 profiles before and after assimilation in BASCOE, Atmos. Chem. Phys., 7, 377–396, 2007, http://www.atmos-chem-phys.net/7/377/2007/. 2463, 2464, 2488
von Clarmann, T.: Validation of remotely sensed profiles of atmospheric state variables: strategies and terminology, Atmos. Chem. Phys., 6, 4311–4320, 2006, http://www.atmos-chem-phys.net/6/4311/2006/. 2444
von Clarmann, T., Ceccherini, S., Doicu, A., Dudhia, A., Funke, B., Grabowski, U., Hilgers, S., Jay, V., Linden, A., López-Puertas, M., Martín-Torres, F. J., Payne, V., Reburn, J., Ridolfi, M., Schreier, F., Schwarz, G., Siddans, R., and Steck, T.: A blind test retrieval experiment for infrared limb emission spectrometry, J. Geophys. Res., 108, 4746, doi: 10.1029/2003JD003835, 2003. 2449
von König, M., Bremer, H., Eyring, V., Goede, A., Hetzheim, H., Kleipool, Q., Küllmann, H., and Künzi, K.: An airborne submm radiometer for the observation of stratospheric trace gases: Microwave Radiometry and Remote Sensing of the Earth's Surface and Atmosphere, Tech. rep., VSP, 409–415, 2000. 2455
Wagner, G. and Birk, M.: New infrared spectroscopic database for chlorine nitrate, J. Quant. Spectrosc. Ra., 82, 443–460, 2003. 2453, 2464
Waibel, A. E., Peter, T., Carslaw, K. S., Oelhaf, H., Wetzel, G., Crutzen, P. J., P´oschl, U., Tsias, A., Reimer, E., and Fischer, H.: Arctic ozone loss due to denitrification, Science, 283, 2064–2068, 1999. 2434
Wang, D. Y., Höpfner, M., Blom, C. E., Ward, W. E., Fischer, H., Blumenstock, T., Hase, F., Keim, C., Liu, G. Y., Mikuteit, S., Oelhaf, H., Wetzel, G., Cortesi, U., Mencaraglia, F., Bianchini, G., Redaelli, G., Pirre, M., Catoire, V., Huret, N., Vigouroux, C., De Mazière, M., Mahieu, E., Demoulin, P., Wood, S., Smale, D., Jones, N., Nakajima, H., Sugita, T., Urban, J., Murtagh, D., Boone, D. J., Bernath, P. F., Walker, K. A., Kuttippurath, J., Kleinböhl, A., Toon, G., and Piccolo, C.: Validation of MIPAS HNO_3 operational data, Atmos. Chem. Phys., 7, 4905–4934, 2007a. 2435, 2436, 2449, 2450, 2464, 2467
Wang, D. Y., Höpfner, M., Mengistu Tsidu, G., Stiller, G. P., von Clarmann, T., Fischer, H., Blumenstock, T., Glatthor, N., Grabowski, U., Hase, F., Kellmann, S., Linden, A., Milz, M., Oelhaf, H., Schneider, M., Steck, T., Wetzel, G., López-Puertas, M., Funke, B., Koukouli,

M. E., Nakajima, H., Sugita, T., Irie, H., Urban, J., Murtagh, D., Santee, M. L., Toon, G., Gunson, M. R., Irion, F. W., Boone, C. D., Walker, K., and Bernath, P. F.: Validation of nitric acid retrieved by the IMK-IAA processor from MIPAS/ENVISAT measurements, Atmos. Chem. Phys., 7, 721–738, 2007b. 2435, 2436, 2446, 2449, 2450, 2467

Waters, J. W., Froidevaux, L., Harwood, R. S., Jarnot, R. F., Pickett, H. M., Read, W. G., Siegel, P. H., Cofield, R. E., Filipiak, M. J., Flower, D. A., Holden, J. R., Lau, G. K., Livesey, N. J., Manney, G. L., Pumphrey, H. C., Santee, M. L., Wu, D. L., Cuddy, D. T., Lay, R. R., Loo, M. S., Perun, V. S., Schwartz, M. J., Stek, P. C., Thurstans, R. P., Boyles, M. A., Chandra, K. M., Chavez, M. C., Gun-Shing, C., Chudasama, B. V., Dodge, R., Fuller, R. A., Girard, M. A., Jiang, J. H., Yibo, J., Knosp, B. W., LaBelle, R. C., Lam, J. C., Lee, K. A., Miller, D., Oswald, J. E., Patel, N. C., Pukala, D. M., Quintero, O., Scaff, D. M., Snyder, W. V., Tope, M. C., Wagner, P. A., and Walch, M. J.: The Earth Observing System Microwave Limb Sounder (EOS MLS) on the Aura Satellite, IEEE Trans. Geosci. Remote Sens., 44, 1075–1092, doi: 10.1109/TGRS.2006.873771, 2006. 2434, 2435, 2447

Wetzel, G., Oelhaf, H., Friedl-Vallon, F., Kleinert, A., Lengel, A., Maucher, G., Nordmeyer, H., Ruhnke, R., Nakajima, H., Sasano, Y., Sugita, T., and Yokota, T.: Intercomparison and validation of ILAS-II version 1.4 target parameters with MIPAS-B measurements, J. Geophys. Res., 111, D11S06, doi:10.1029/2005JD006287, 2006. 2435, 2436

Yokota, T., Nakajima, H., Sugita, T., Tsubaki, H., Itou, Y., Kaji, M., Suzuki, M., Kanzawa, H., Park, J. H., and Sasano, Y.: Improved Limb Atmospheric Spectrometer (ILAS) data retrieval algorithm for Version 5.20 gas profile products, J. Geophys. Res., 107, 8216, doi:10.1029/2001JD000628, 2002. 2436

Zander, R. and Demoulin, P.: Spectroscopic evidence for the presence of the ν_4-Q branch of chlorine nitrate ($ClONO_2$) in ground-based infrared solar spectra, J. Atmos. Chem., 6, 191–200, 1988. 2435

Zander, R., Rinsland, C. P., Farmer, C. B., Brown, L. R., and Norton, R. H.: Observation of several chlorine nitrate ($ClONO_2$) bands in stratospheric infrared spectra, Geophys. Res. Lett., 13, 757–760, 1986. 2435

Zander, R., Mahieu, E., Gunson, M. R., Abrams, M. C., Chang, A. Y., Abbas, M., Aellig, C., Engel, A., Goldman, A., Irion, F. W., Kampfer, N., Michelsen, H. A., Newchurch, M. J., Rinsland, C. P., Salawitch, R. J., Stiller, G. P., and Toon, G. C.: The 1994 northern midlatitude budget of stratospheric chlorine derived from ATMOS/ATLAS-3 observations, Geophys. Res. Lett., 23, 2357–2360, 1996. 2435

Zander, R., Mahieu, E., Demoulin, P., Duchatelet, P., Roland, G., Servais, C., Mazière, M. D., Reimann, S., P., C., and Rinsland: Our changing atmosphere: evidence based on long-term infrared solar observations at the Jungfraujoch since 1950, Sci. Tot. Environ., 391, 184–195, 2007. 2488

Table 1. Summary of the correlative datasets used in the statistical and individual profile comparisons with ACE-FTS HNO_3, $ClONO_2$, and N_2O_5.

Instrument (Retrieval Code)	Comparison Period	Comparison Location	Vertical Range and Resolution	Coincidence Criteria	Number of Coincidences	Species
SMR (Chalmers v2.0)	2004/02/21 – 2006/11/30	85° S– 86° N	18–45 km at 1.5–2.0 km	±12 h, 500 km	1571	HNO_3
MLS (v2.2)	2004/09/15 – 2007/05/22	82° S– 82° N	215–3.2 hPa at 3.5–5.5 km	±12 h, ±1° lat., ±8° long	7178	HNO_3
MIPAS (ESA v.4.62)	2004/02/21 – 2004/03/26	20° N– 85° N	6–68 km at 3 km	±6 h, 300 km	138	HNO_3
MIPAS (IMK-IAA[b])	2004/02/21 – 2004/03/25	30° N– 90° N	6–60 km at 3–8 km	±9 h, 800 km[a]	575 580 574	HNO_3 v.8[b] $ClONO_2$ v.11[b] N_2O_5 v.9[b]
ASUR	2005/01/24 – 2005/02/07	60° N– 70° N	18–46 km at 8–16 km	±12 h, 1000 km	16	HNO_3
SPIRALE	2006/01/20	67.6° N, 21.55° E	15–26 km at several m	−13 h, 413 km	1	HNO_3
FIRS-2	2007/01/24	67.27° N, 27.29° E	13–31 km at 1 km	+26 h 481 km	1 1 1	HNO_3 $ClONO_2$ N_2O_5

[a] Additional PV criteria: $3\times10^{-6}\,Km^2\,kg^{-1}\,s^{-1}$ at 475 K
[b] Different retrieval versions were used for each species

ACPD
8, 2429–2512, 2008

Table 2. The ground-based FTIR stations contributing HNO_3 and $ClONO_2$ partial columns for comparisons with ACE-FTS. The locations (latitude, longitude, and altitude in m above sea level a.s.l.) are listed, along with the instrument manufacturer and model, the nominal spectral resolution, the retrieval code, and microwindows (MW) used to derive HNO_3 and $ClONO_2$ partial columns, and references that provide additional details regarding the stations and for the measurements used here.

Station Reference	Location	Alt. [m a.s.l.]	Instrument	Res'n [cm^{-1}]	Retrieval Code	HNO_3 MW [cm^{-1}]	$ClONO_2$ MW [cm^{-1}]
Thule F Goldman et al. (1999)	76.5° N 68.7° W	225	Bruker 120M	0.004	SFIT2 3.92b	867.50–870.00	780.12–780.32 780.70–781.25[a]
Kiruna Blumenstock et al. (2006)	67.8° N 20.4° E	419	Bruker 120HR	0.005	PROFFIT92	867.00–869.60, 872.80–875.20	780.05–780.355 779.30–780.60[a]
Poker Flat Kasai et al. (2005)	65.1° N 147.4° W	610	Bruker 120HR	0.007	SFIT2 3.7	867.45–869.25	no comparison data
Jungfraujoch Mahieu et al. (1997) Zander et al. (2007)	46.5° N 8.0° E	3580	Bruker 120HR	0.004 or 0.006	SFIT2 3.91	868.50–870.00	780.05–780.355 779.30–780.60[a]
Izaña Schneider et al. (2005)	28.3° N 16.5° W	2367	Bruker 120M Bruker 125HR[b]	0.005	PROFFIT92	867.00–869.60, 872.80–875.20	no comparison data
Reunion Island Senten et al. (2007)	20.9° S 55.5° E	50	Bruker 120M	0.005	SFIT2 3.92	872.25–874.80	no comparison data
Wollongong Paton-Walsh et al. (2005)	34.5° S 150.9° E	30	Bomem DA8	0.004	SFIT2 3.92	868.50–870.00, 872.80–874.00	780.050–780.355 779.30–780.60[a]
Lauder Griffith et al. (2003) Vigouroux et al. (2007)	45.0° S 169.7° E	370	Bruker 120HR	0.0035	SFIT2 3.82	866.30–859.60 872.80–874.00	no comparison data
Arrival Heights Goldman et al. (1999) Vigouroux et al. (2007)	77.8° S 166.65° E	200	Bruker 120M	0.0035	SFIT2 3.82	868.30–869.60 872.80–874.00	no comparison data

[a] The wider microwindow is used for retrieving H_2O, CO_2, and O_3. In a second step, $ClONO_2$ is retrieved using this results.

[b] The Bruker 120M was used until December 2004 at Izaña. The Bruker 125HR has been in use since January 2005.

ACPD
8, 2429–2512, 2008

Table 3. Summary of the results of the HNO_3 partial column comparisons between ACE-FTS and the ground-based FTIR stations. *N* is the number of coincidences, DOFS is the degrees of freedom for signal for the FTIR partial columns over the given altitude range of the comparison. The mean relative difference is calculated as 100% × the mean of the *N* differences (ACE-FTS–FTIR)/FTIR, and is given along with the standard deviation on the ensemble, and the standard error on the mean.

Station	Latitude	Coincidence Criteria [km, h]	*N*	Partial Column Altitude Range [km]	Partial Column DOFS	Relative Difference [%]	Standard Deviation [%]	Standard Error [%]
Thule	76.5° N	500, ±12	14	14.6–30.2	1.9	2.4	5.8	1.6
Kiruna	67.8° N	500, ±12	20	16.0–29.1	1.6	2.5	9.7	1.8
Poker Flat	65.1° N	1000, ±24	5	15.0–29.0	2.2	−11.4	19.5	8.7
Jungfraujoch	46.5° N	1000, ±24	26	15.0–31.0	1.4	0.7	13.0	2.5
Izaña	28.3° N	1000, ±24	9	16.0–29.1	1.7	−2.0	23.7	7.9
Reunion Island	20.9° S	1211[a], ±24	5	16.0–29.2	1.0	−6.2	23.9	10.7
Wollongong	34.5° S	1000, ±24	7	15.0–29.0	1.6	6.0	24.8	9.4
Lauder	45.0° S	1000, ±24	19	15.0–29.0	2.1	−0.9	21.5	4.9
Arrival Heights	77.8° S	1000, ±24	17	15.0–29.0	2.0	−12.6	59.2	14.4

[a] coincidence criteria for Reunion Island: 15° longitude, 10° latitude, and 24 h

ACPD
8, 2429–2512, 2008

EGU

Table 4. Same as Table 3, but for $ClONO_2$

Station	Latitude	Coincidence Criteria [km, h]	*N*	Partial Column Altitude Range [km]	Partial Column DOFS	Mean Relative Difference [%]	Standard Deviation [%]	Standard Error [%]
Thule	76.5° N	500, ±12	11	18.2–30.2	0.9	−1.0	28.9	8.7
Kiruna	67.8° N	500, ±12	29	16.0–29.1	0.9	34.3	25.6	4.7
Jungfraujoch	46.5° N	1000, ±24	15	19.0–40.0	1.0	4.7	16.3	4.2
Wollongong	34.5° S	1000, ±24	7	15.0–29.0	0.3	14.6	30.8	11.6

Table 5. Summary of results of the statistical profile comparisons for HNO_3, $ClONO_2$ and N_2O_5 between ACE-FTS and the correlative measurements.

Instrument (Data Product)	Number of Events	Altitude Range [km]	Absolute Differences: Typical [ppbv]	Absolute Differences: Maximum [ppbv]	Relative Differences: Typical [%]	Relative Differences: Maximum [%]
			HNO_3			
SMR[a] v2.0	1571	18–35	−1.00	−1.90	−20	−25
MLS v2.2	7178	18–32	+0.60	+0.80	+13	+23
MIPAS	138	10–27	−0.10	−0.50	±2	−5
(ESA v4.62)		27–36	−0.10	−0.70	±9	−25
MIPAS	575	10–31	−0.20	−0.70	±2	+9
(IMK-IAA v8)		31–35	+0.20	+0.30	+11	+17
ASUR	16	18–26	+1.50	+2.50	+20	+32
		26–36	±0.20	−0.30	±3	−6
SPIRALE	1	15–26	+2.40	+4.20	+28	+45
FIRS-2	1	13–31	±2.00	±3.00	±20	−55
			$ClONO_2$			
MIPAS[b]	580	16–27	±0.01	−0.04	±1	−6
(IMK-IAA v11)		27–34	+0.09	+0.13	+14	+22
FIRS-2	1	14–31	−1.00	−2.80	–	–
			N_2O_5			
MIPAS daytime[b]	275	16–27	±0.02	+0.04	−10	−36
(IMK-IAA v9)		27–34	−0.14	−0.25	−28	−44
MIPAS nighttime[b]	299	16–27	−0.05	−0.09	−27	−52
(IMK-IAA v9)		27–33	−0.17	−0.22	−36	−48
FIRS-2	1	27–31	−0.30	−0.60	−25	−51

[a] SMR data shifted upwards by 1.5 km (see text).
[b] CTM-corrected results for MIPAS (see text).

ACPD
8, 2429–2512, 2008

EGU

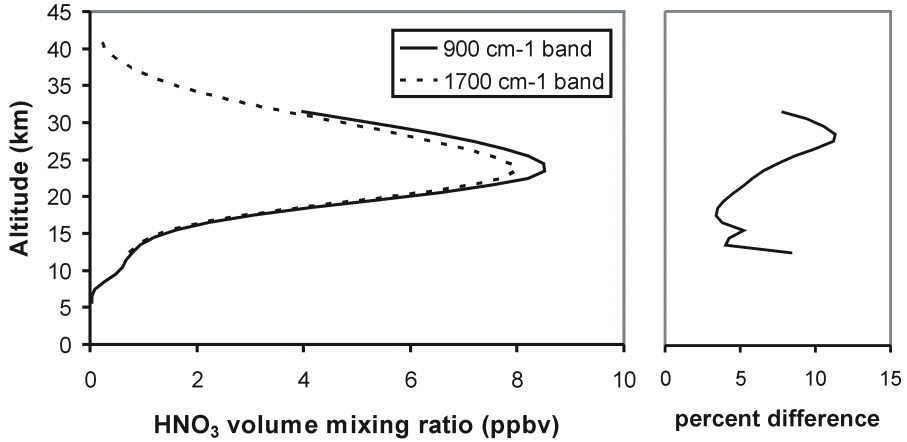

Fig. 1. Comparison of ACE-FTS HNO_3 profiles using two different sets of microwindows. Left panel: Retrieved HNO_3 mean VMR profiles (averaged over 100 profiles) using the 900 cm^{-1} and 1700 cm^{-1} wavenumber regions. Right panel: Relative differences calculated as [HNO_3(900)–HNO_3(1700)]/HNO_3 (900) as percentage.

ACPD
8, 2429–2512, 2008

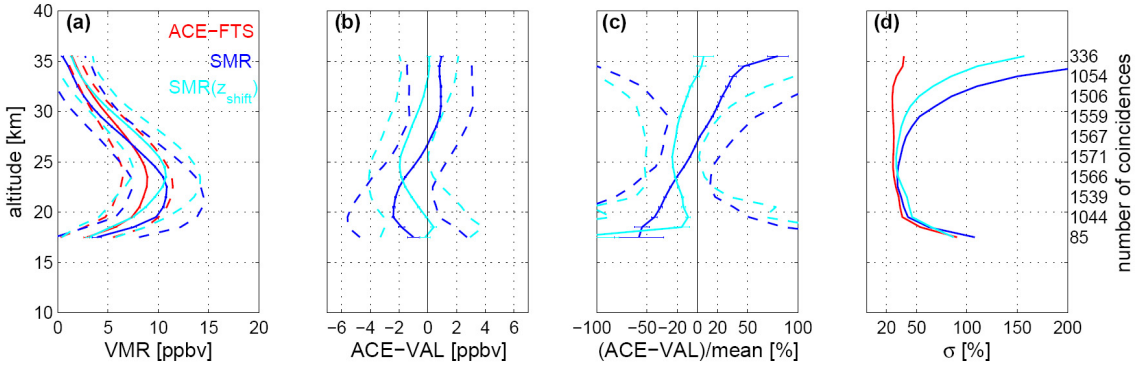

Fig. 2. Comparison of HNO_3 profiles from ACE-FTS and SMR and for all coincidences between 85° S–86° N (±12 h, 500 km). **(a)** Mean profiles for ACE-FTS (red solid line), SMR (blue solid line), and SMR shifted upwards by 1.5 km (cyan solid line). Their $\pm 1\sigma$ standard deviations are plotted as dashed lines, and the standard errors in the mean ($\sigma/\sqrt{N}$) are included as error bars on the mean profiles. **(b)** Mean absolute difference profile (solid lines) with $\pm 1\sigma$ standard deviation (dashed lines) and the standard error in the mean (error bars). **(c)** Profile of the mean relative differences, as percentage, calculated using Eq. (2) (solid lines) with $\pm 1\sigma$ standard deviation (dashed lines). Standard errors are included as error bars. **(d)** Relative standard deviations on the mean profiles shown in (a). The number of coincident pairs at selected altitudes is given on the right-hand y-axis.

ACPD
8, 2429–2512, 2008

EGU

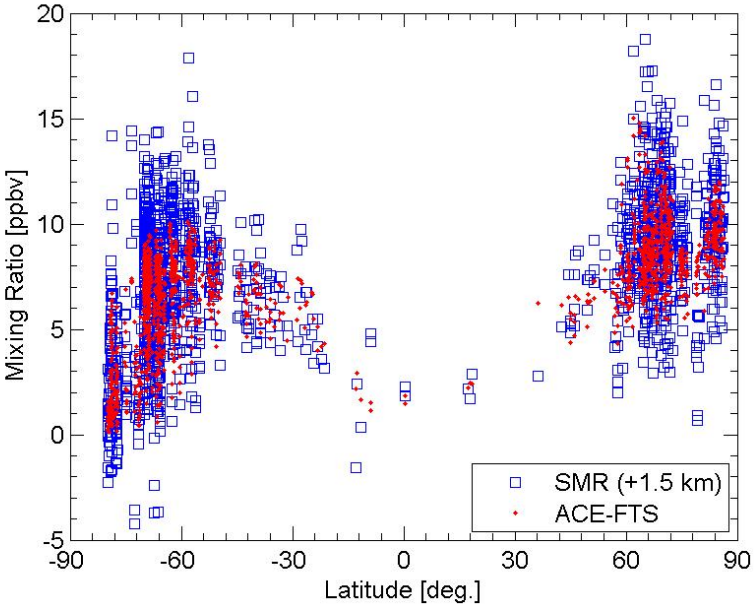

Fig. 3. Individual ACE-FTS and SMR coincident data points as a function of latitude for September-October-November 2004–2006 and altitudes between 18 and 22 km. The SMR data is shown with the +1.5 km shift in altitude applied.

ACPD
8, 2429–2512, 2008

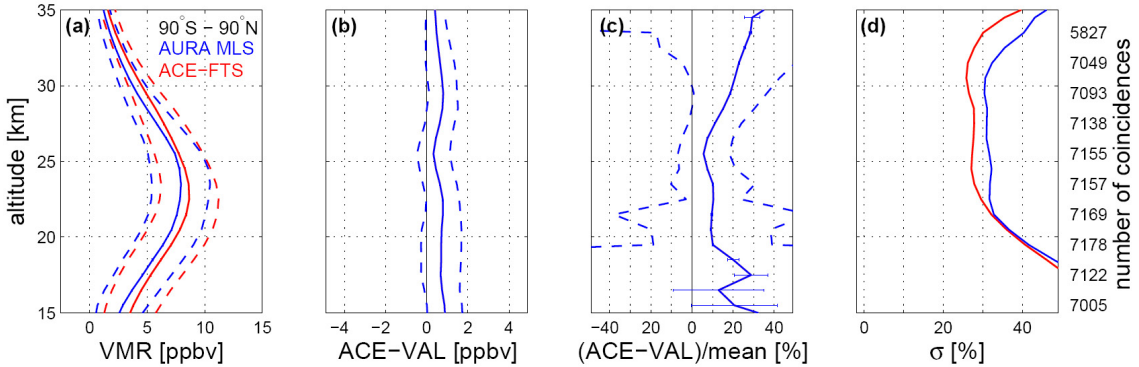

Fig. 4. Same as Fig. 2 but for HNO_3 comparisons between ACE-FTS and MLS for all coincidences between 82° S and 82° N (±12 h, ±1° lat., ±8° long.).

ACPD
8, 2429–2512, 2008

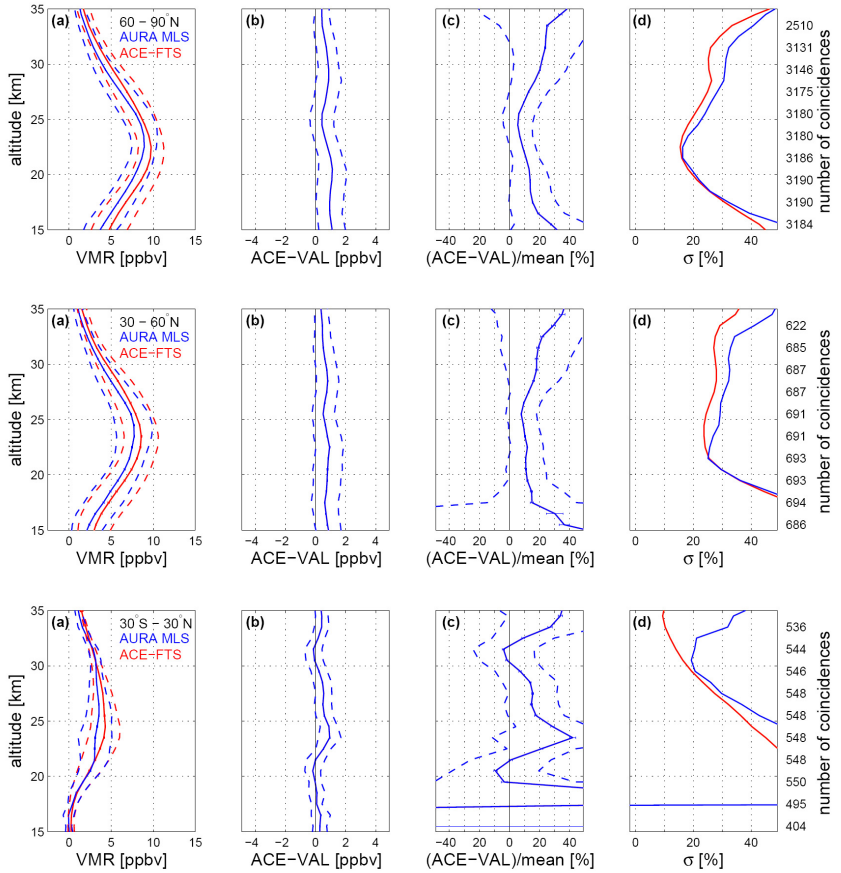

Fig. 5. Part 1: Same as Fig. 2 but for HNO_3 comparisons between ACE-FTS and MLS for different latitude bands (±12 h, ±1° lat., ±8° long). Top row: 60–90° N, middle row: 30–60° N, bottom row: 30° S–30° N.

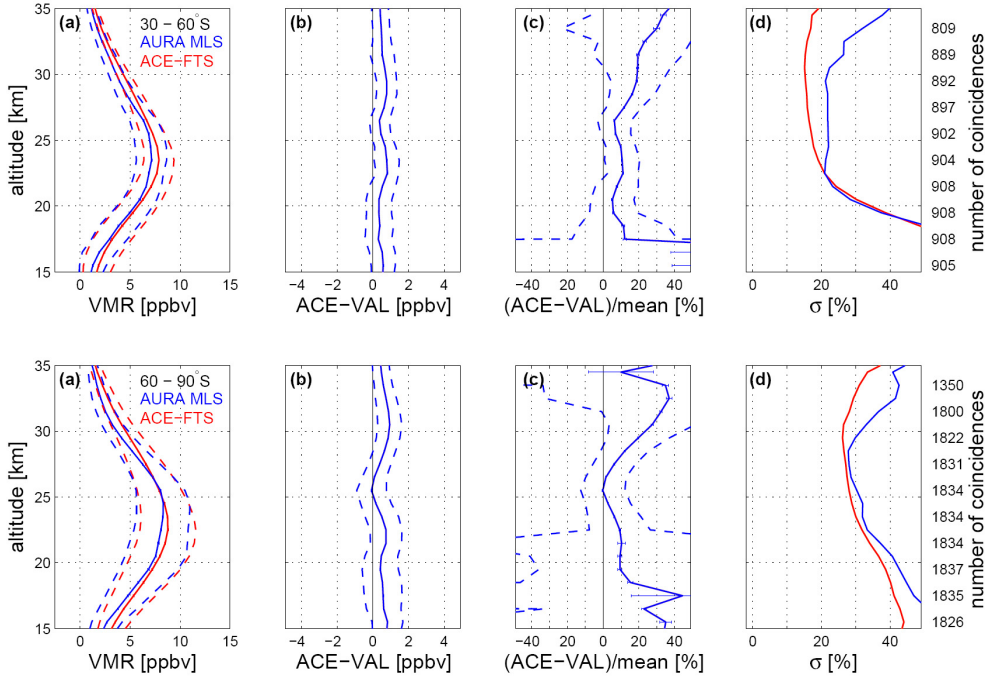

Fig. 5. Continued (Part 2). Top row: 30–60° S, bottom row: 60–90° S.

ACPD
8, 2429–2512, 2008

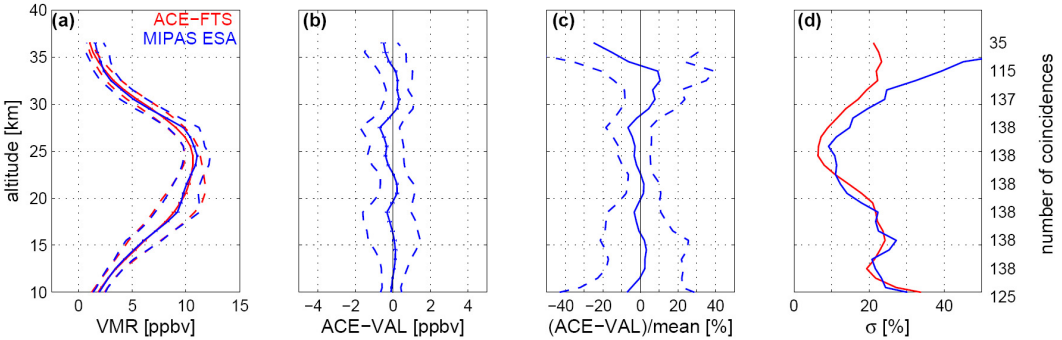

Fig. 6. Same as Fig. 2 but for HNO_3 comparison between ACE-FTS and the MIPAS ESA data product for coincident measurements between 20° N and 85° N (±6 h, 300 km).

ACPD
8, 2429–2512, 2008

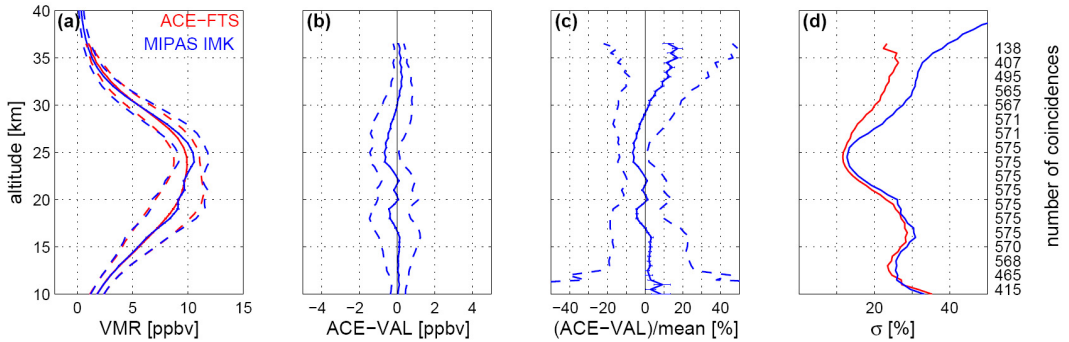

Fig. 7. Same as Fig. 2 but for HNO_3 comparison between ACE-FTS and the MIPAS IMK-IAA data product for coincident measurements between 30° N–90° N(±9 h, 800 km, $\pm 3 \times 10^{-6}$ K m^2 kg^{-1} s^{-1} at 475 K).

ACPD
8, 2429–2512, 2008

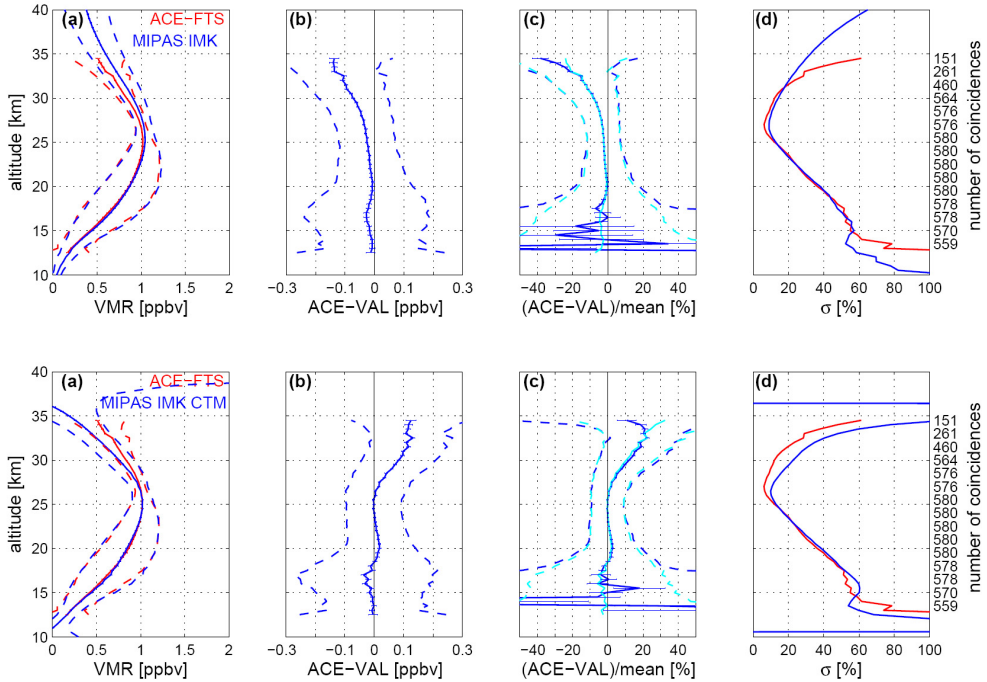

Fig. 8. Same as Fig. 2 but for $ClONO_2$ comparisons between ACE-FTS and the MIPAS IMK-IAA data product for coincident measurements between 30° N–90° N (±9 h, 800 km, $\pm 3\times10^{-6}$ K m^2 kg^{-1} s^{-1} at 475 K). Panels (c) also show the mean relative deviation from the mean, calculated using Eq. (4) (cyan solid line) with $\pm1\sigma$ relative standard deviation (cyan dashed line). Top row: MIPAS uncorrected data. Bottom row: MIPAS CTM-corrected data.

ACPD
8, 2429–2512, 2008

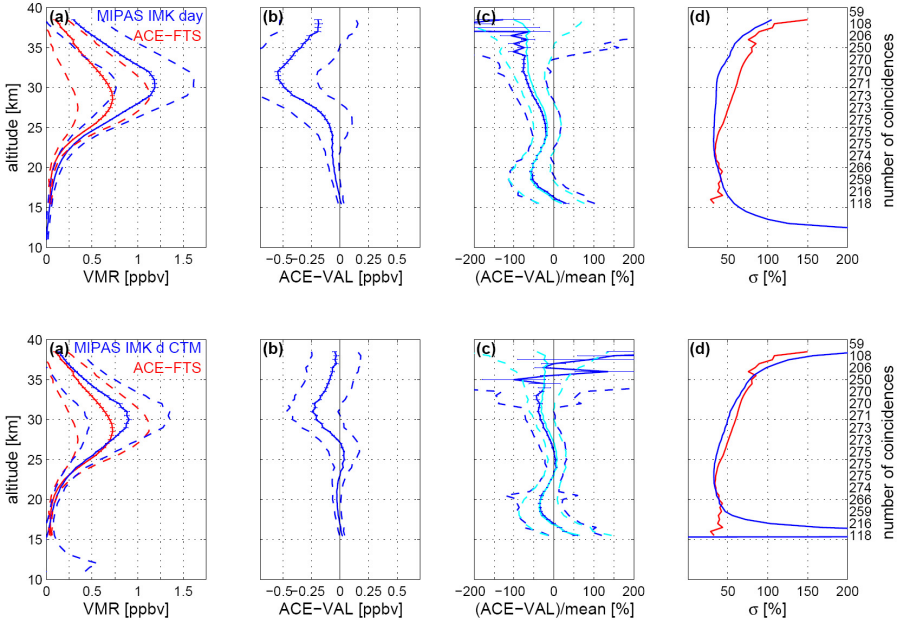

Fig. 9. Same as Fig. 2 but for N_2O_5 comparisons between ACE-FTS and MIPAS IMK-IAA data product for coincident measurements between 30° N–90° N (±9 h, 800 km, $\pm 3\times10^{-6}$ K m^2 kg^{-1} s^{-1} at 475 K). Panels (c) also show the mean relative deviation from the mean, calculated using Eq. (4) (cyan solid line) with $\pm1\sigma$ relative standard deviation (cyan dashed line). First row: MIPAS daytime measurements; second row: CTM-corrected MIPAS daytime measurements; third row: MIPAS nighttime measurements; fourth row: CTM-corrected MIPAS nighttime measurements.

ACPD
8, 2429–2512, 2008

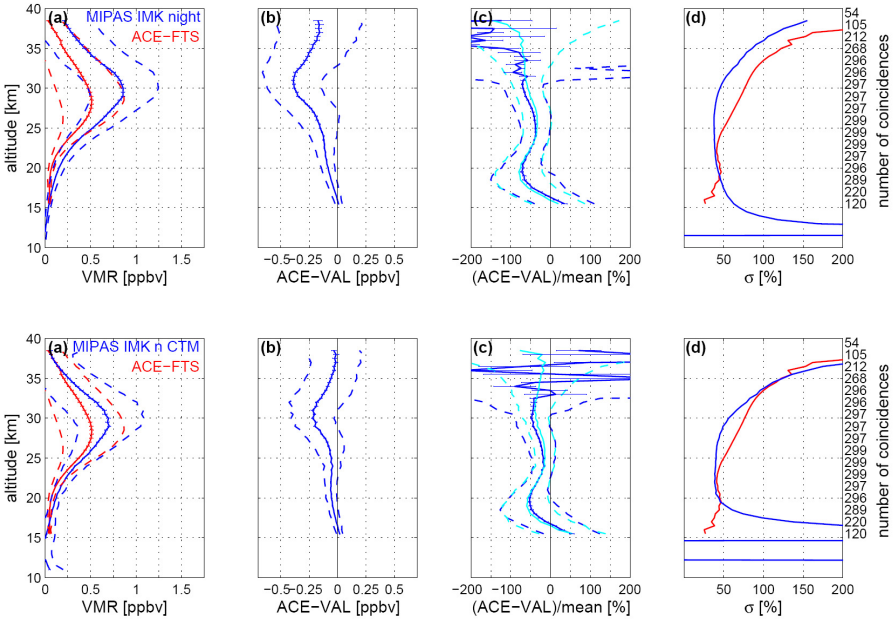

Fig. 9. Continued.

ACPD
8, 2429–2512, 2008

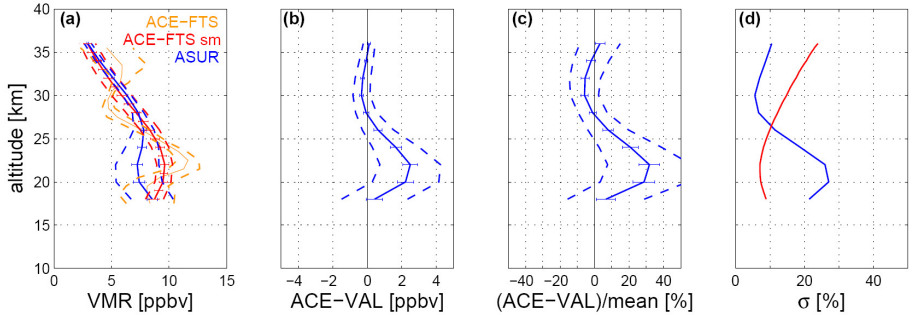

Fig. 10. Same as in Fig. 2 for HNO_3 comparisons between ACE-FTS and ASUR for 16 coincidences between 60° N and 70° N, (±12 h, 1000 km) except that in panel (a) the original ACE-FTS profile is now plotted in orange and the ACE-FTS profile smoothed by the ASUR averaging kernels is plotted in red. The smoothed ACE-FTS profile is used for the comparison results shown in panels (a), (c).

ACPD
8, 2429–2512, 2008

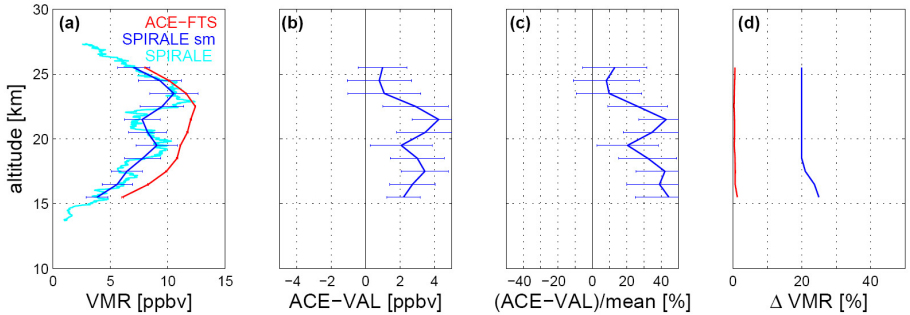

Fig. 11. (a) Single HNO_3 vertical profiles obtained by SPIRALE on 20 January 2006 and during ACE-FTS occultation sr13151 on 21 January 2006 (red). The cyan line corresponds to the original SPIRALE measurements and the blue line corresponds to the SPIRALE profile smoothed with a triangular function (see text). Uncertainties are shown as error bars on both profiles. **(b)** Absolute difference profile (solid line) with error bars representing the combined random error, computed as the root-sum-square error of the ACE-FTS fitting error and the SPIRALE uncertainty. **(c)** Relative difference profile, as a percentage with error bars representing the relative combined random error. **(d)** The relative values of the ACE-FTS fitting error (red) and the SPIRALE uncertainty (blue).

ACPD
8, 2429–2512, 2008

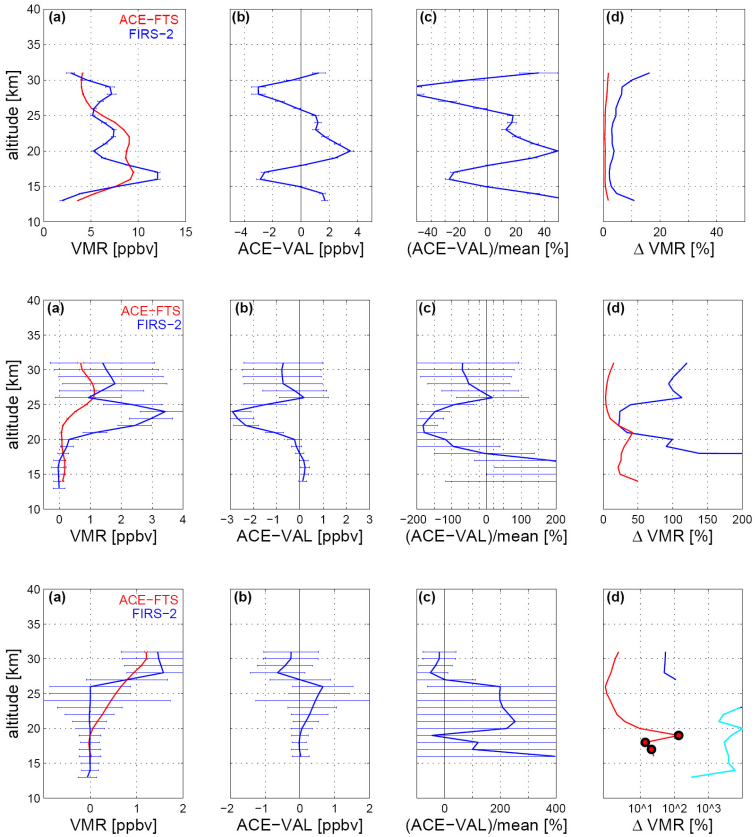

Fig. 12. Same as Fig. 11, but for the comparisons between the FIRS-2 balloon flight on 24 January 2007 and ACE occultation sr18561 on 23 January 2007. (Top row) HNO_3 measurements. (Middle row) $ClONO_2$ measurements. (Bottom row) N_2O_5 measurements: Note the logarithmic scale in panel (d). Negative fractional uncertainties in panel (d) are plotted positive and are marked: red circles for negative ACE-FTS fractional uncertainties and cyan lines for negative FIRS-2 fractional uncertainties.

ACPD
8, 2429–2512, 2008

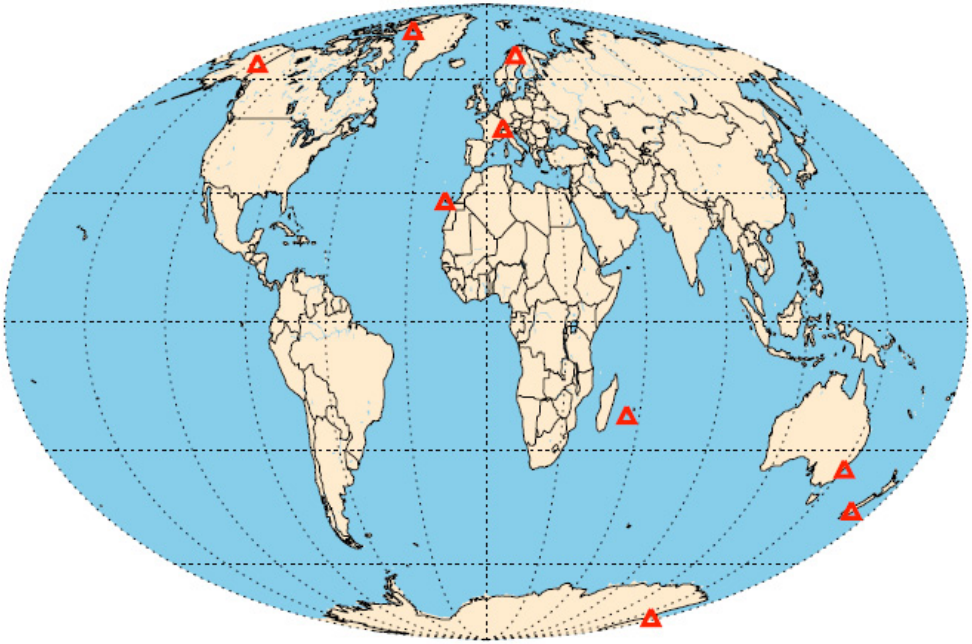

Fig. 13. Geographic locations of the nine ground-based FTIR validation instruments used in this paper.

ACPD

8, 2429–2512, 2008

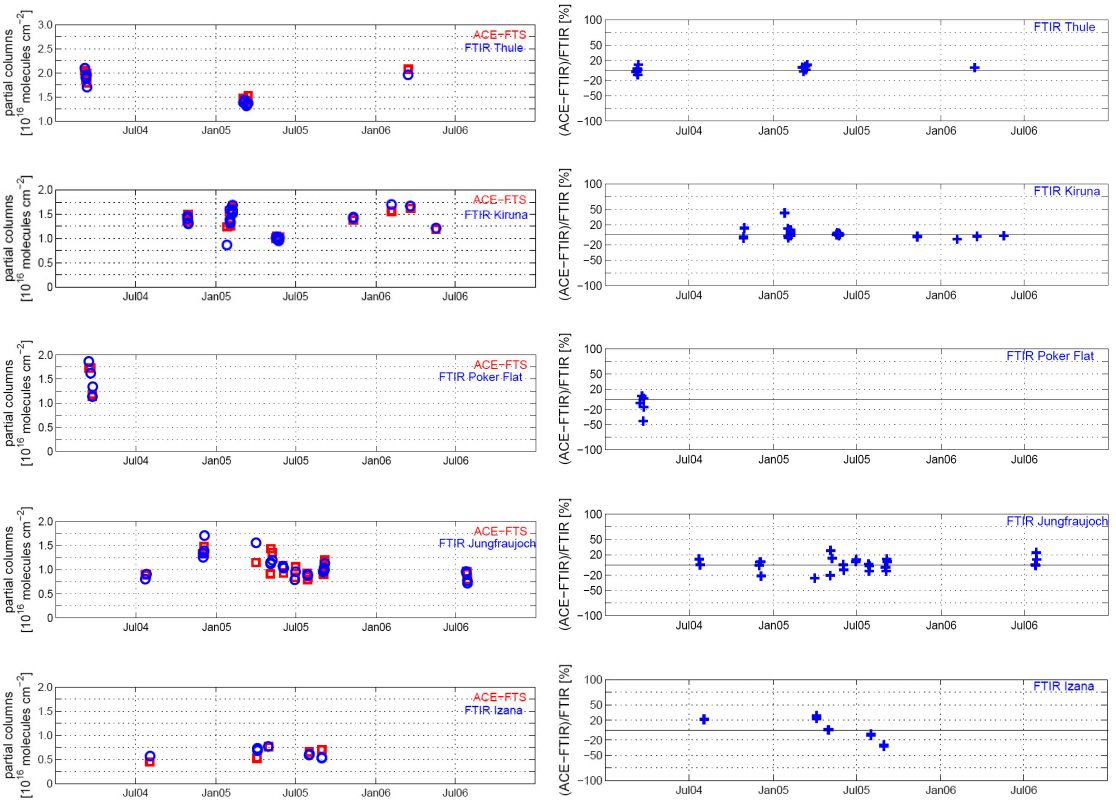

Fig. 14. Comparison of ACE-FTS and ground-based FTIR HNO_3 partial columns. For each station, the left-hand panel shows the time series of partial columns from ACE-FTS (red squares) and the FTIR (blue circles), and the right-hand panel shows the relative differences as a percentage of the FTIR partial columns. Note that the y-axis scales is different for Thule FTIR in the left hand panel.

ACPD
8, 2429–2512, 2008

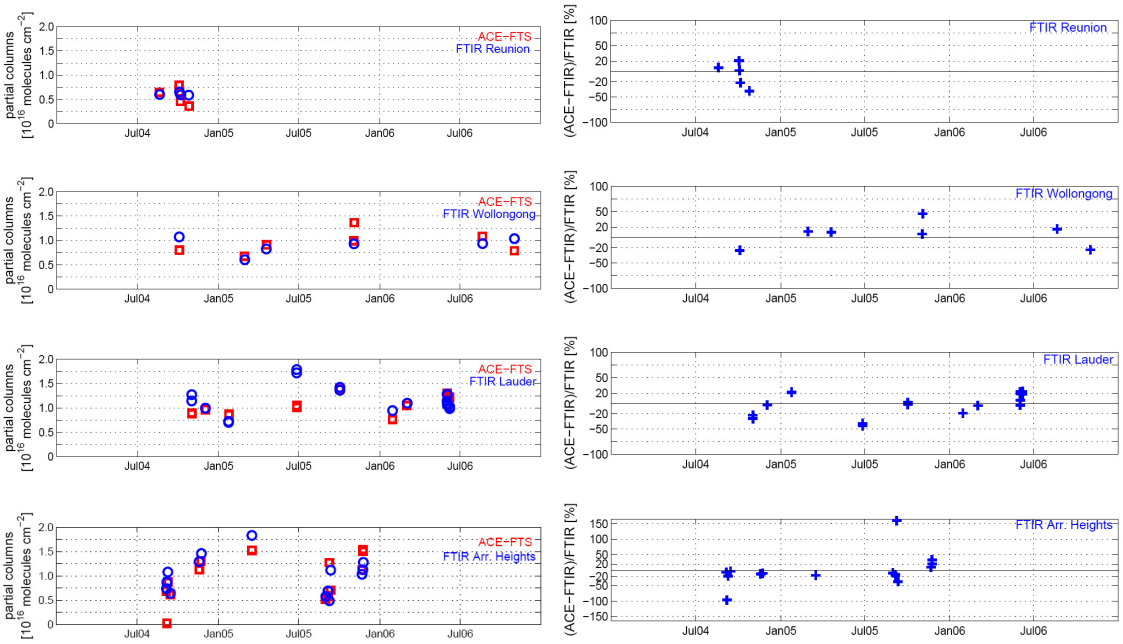

Fig. 14. Continued.

ACPD
8, 2429–2512, 2008

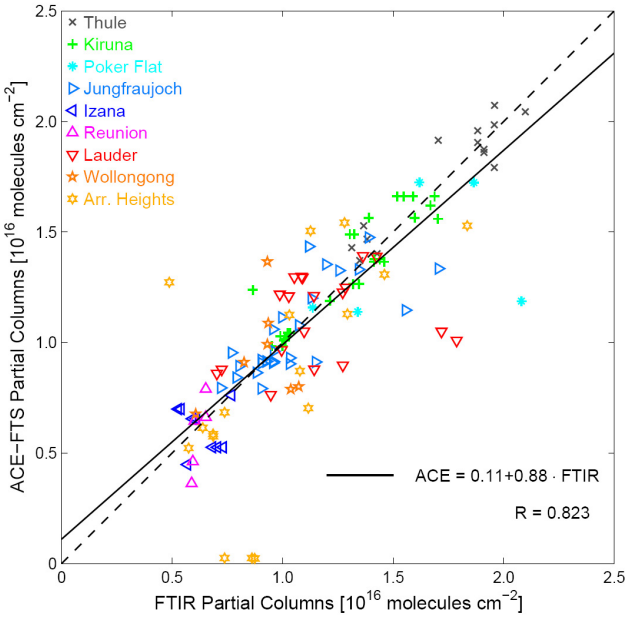

Fig. 15. Scatter plot of the ACE-FTS and ground-based FTIR HNO_3 partial columns shown in Fig. 14. The solid black line is the least-squares linear fit to the data, with the slope, intercept and correlation coefficient given in the figure. The dashed line shows the one-to-one relationship.

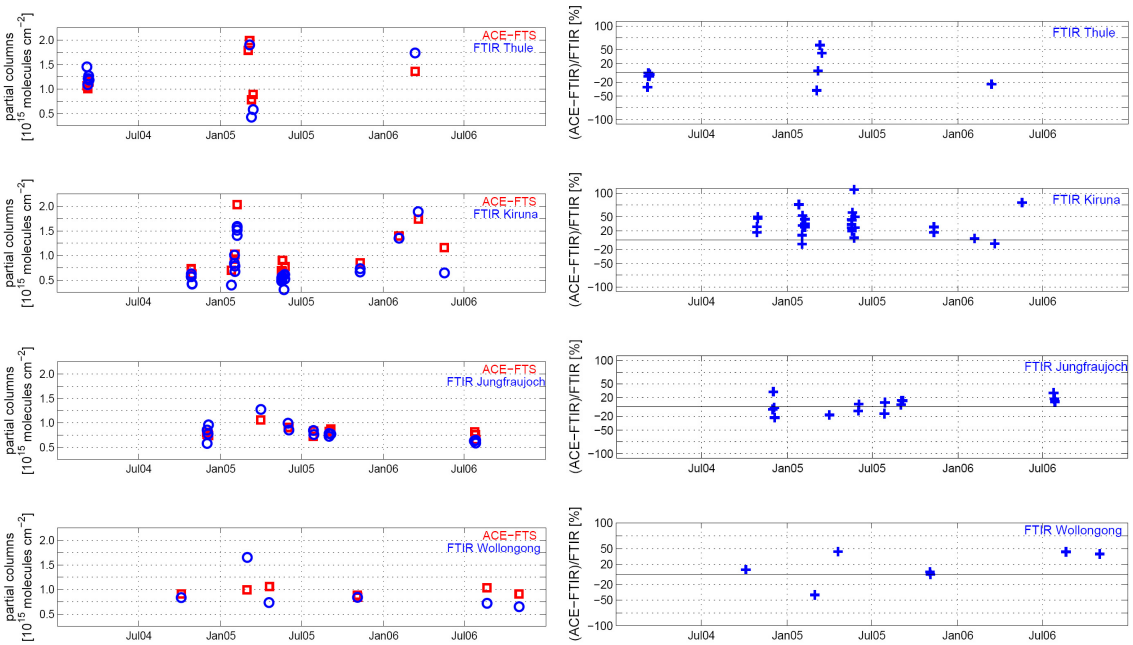

Fig. 16. Same as Fig. 14 for $ClONO_2$.

ACPD
8, 2429–2512, 2008

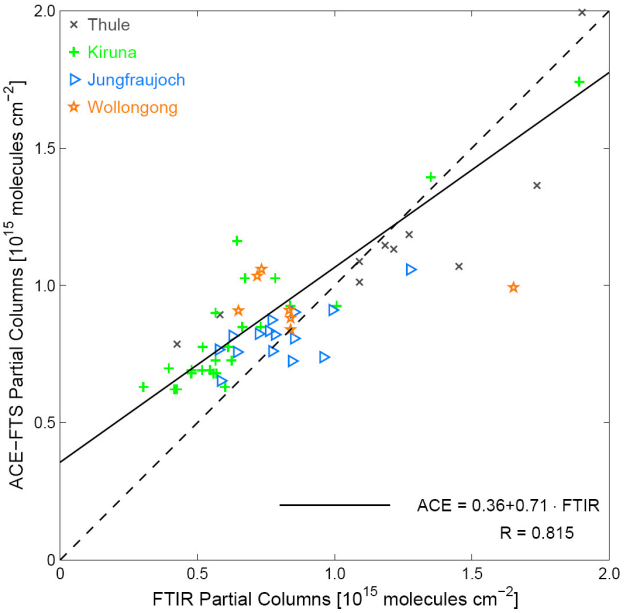

Fig. 17. Scatter plot of the ACE-FTS and ground-based FTIR $ClONO_2$ partial columns shown in Fig. 16. The solid black line is the least-squares linear fit to the data, with the slope, intercept and correlation coefficient given in the figure. The dashed line shows the one-to-one line relationship.

ACPD
8, 2429–2512, 2008

EGU

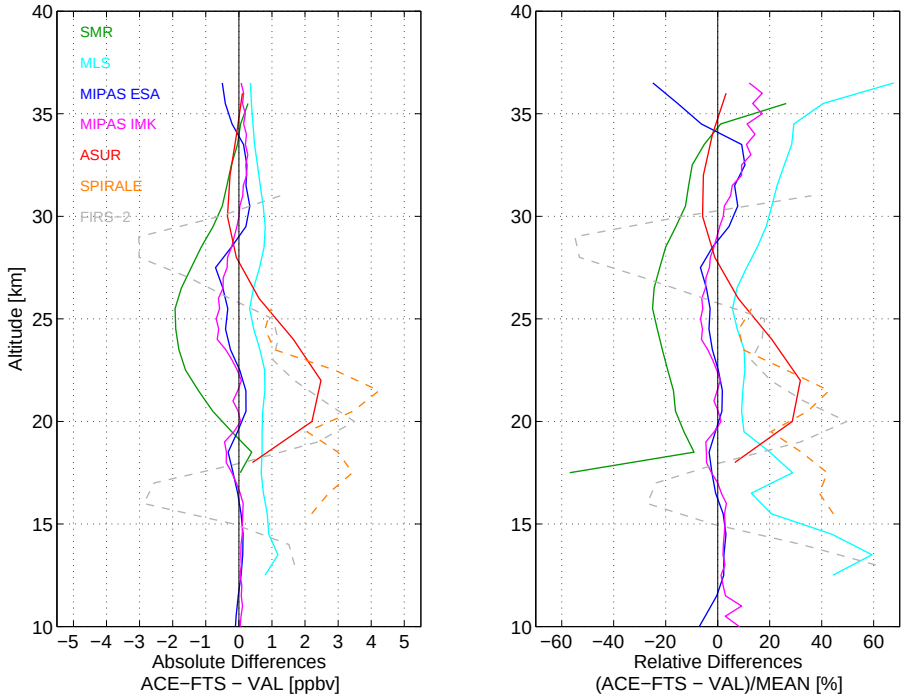

Fig. 18. Summary plots for all of the VMR comparisons with ACE-FTS HNO_3. Left panel: Profiles of the mean absolute difference. Right panel: Profiles of the relative differences. In both panels, the statistical comparisons are indicated by solid lines, and the individual profile comparisons are indicated by the dashed lines.

ACPD
8, 2429–2512, 2008